Article

Synthesis and Characterization of Thiophosphoramidate Morpholino Oligonucleotides and Chimeras

Heera K Langner, Katarzyna Jastrzebska, and Marvin H. Caruthers

J. Am. Chem. Soc., **Just Accepted Manuscript** • DOI: 10.1021/jacs.0c04335 • Publication Date (Web): 31 Aug 2020

Synthesis and Characterization of Thiophosphoramidate Morpholino Oligonucleotides and Chimeras.

Heera K. Langner*, Katarzyna Jastrzebska†, Marvin H. Caruthers*

Department of Chemistry and Biochemistry, University of Colorado at Boulder, Boulder, Colorado 80309, United States

ABSTRACT: This manuscript outlines the optimized chemical synthesis and preliminary biochemical characterization of a new oligonucleotide analogue called thiophosphoramidate morpholinos (TMOs). Their rational design hinges upon integrating two well-studied pharmacophores, namely phosphorothioates (pS) and morpholinos, to create morpholino-pS hybrid oligonucleotides. Our simple synthesis strategy enables the easy incorporation of morpholino-pS moieties and therapeutically relevant sugar modifications in tandem to create novel oligonucleotide (ON) analogs that are hitherto unexplored in the oligotherapeutics arena. Exclusively TMO modified ONs demonstrate high stability towards 3'-exonuclease. Hybridization studies show that TMO chimeras consisting of alternating TMO and DNA-pS subunits exhibit higher binding affinity towards complementary RNA relative to the canonical DNA/RNA duplex (~10 °C). Oligonucleotides that consist entirely of TMO linkages also show higher RNA binding affinity, but do not recruit RNase H1. Chimeric TMO analogues demonstrate high gene silencing efficacy, comparable to that of a chimeric 2'-OMe-pS/pO control, during *in vitro* bioassay screens designed to evaluate their potential as microRNA inhibitors of hsa-miR-15b-5p in HeLa cells.

Introduction

In this age of personalized medicine, oligonucleotide therapies are emerging as a reliable platform for drug development.[1] Due to their size (between 6-10 kDa) and charge, oligonucleotides (ONs) possess very different pharmacodynamic and pharmacokinetic properties relative to conventional small molecule drugs. While small molecules drugs directly interact with diseased proteins, ON drugs alter the mRNAs that produce these proteins and thereby prevent pathogenesis at a much earlier stage.[2] Synthetic ON drugs can interact specifically with their mRNA target through Watson-Crick base pairing and either force RNA blockade (e.g., antisense-mediated exon-skipping, microRNA inhibition) or irreparably degrade their target (e.g., RNase H1 or Ago2 mediated cleavage) which stops the transfer of genetic information from the mutated gene to the defective protein.[3-4] Their unique modes of action enables them to target the "undruggable" space, which includes several rare genetic disorders for which no therapeutic modalities currently exist.[5]

Depending upon structural design and how they alter protein expression, ON drugs are classified into antisense, siRNA, antagomirs, splice-switching oligonucleotides, aptamers and so on.[6] Over the past four decades, numerous chemical modifications have been developed to modulate various biochemical properties such as binding affinity, nuclease resistance, in vitro and in vivo delivery and to minimize immune stimulation and associated toxicities.[7] Among these analogues, one distinct class of synthetic ONs called phosphorodiamidate morpholinos (PMOs, Figure 1a) has gained substantial interest. Two steric blocker PMO drugs which can access a "difficult to drug" target, namely the mRNA of the human dystrophin gene, have been conditionally approved for the treatment of Duchenne Muscular Dystrophy and two more are under Phase III clinical trials.[8-10] Several oligonucleotide drugs containing the phosphorothioate linkage have also been FDA approved (Vitravene®, Kynamro®, Spinraza®, Tegsedi™, Givlaari™). During their course of development, the clinically relevant pharmacokinetics, biodistribution, metabolism and toxicity profiles of both pS and PMO based ONs have undergone intensive research validation through many years of elaborate testing and clinical trials.[11] These studies have revealed that PMOs exhibit fast plasma clearance and minimal drug related toxicity at clinically relevant doses; however, they also show poor cellular uptake and pharmacokinetics.[12] In contrast, ONs containing pS internucleotide linkages interact with a wide variety of proteins (e.g., plasma proteins) resulting in off-target effects and toxicity.[13] Although they possess superior enzymatic stability, their "stickiness" leads to reduced renal clearance, longer circulation half-lives and good tissue distribution.[14]

Despite their individual successes, the chemical synthesis of oligonucleotide hybrids that incorporate both morpholino and DNA-pS subunits has been hampered by the inherent drawbacks associated with utilizing the P(V) based synthetic strategy that is currently being used to generate PMOs.[15] Additionally, second and third generation sugar

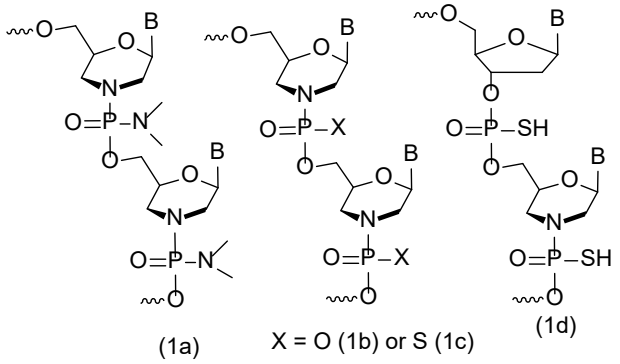

Figure 1 Chemical representation of phosphorodiamidate morpholino (PMO) (1a), phosphoramidate morpholino (1b), thiophosphoramidate morpholino (TMO) (1c) and TMO-DNA-pS chimeras (1d).

modifications such as 2'-OMe, 2'-F, 2'-O-MOE, and LNA[16] are only available as phosphoramidite synthons. Although several PMO hybrids have been synthesized using conventional P(V) chemistry,[17] a robust and flexible synthetic route that would generate chimeras containing morpholino nucleotides in conjunction with therapeutically relevant modifications has yet not been reported. Such chimeric analogues could prove beneficial for developing new therapeutic drugs with biological attributes that are unlike those of their parent pharmacophores.

Towards this goal, previous work has focused on the synthesis of morpholino-DNA chimeras containing various chemical modifications including boranophosphoramidate, phosphoramidate and alkyl phosphoramidate linkages.[18] Other literature examples include morpholino methylphosphonamidates[19] and triazole-linked morpholino analogs.[20] Zhang et al. reported the synthesis and characterization of phosphoramidate morpholino-DNA chimeras (10-12mers) containing up to three morpholino thymidine (mT) phosphoramidate linkages (Figure 1b) and morpholino-RNA chimeras (21 mers) having one or two morpholino uridine (mU) phosphoramidate linkages.[21-22] They reported that the introduction of one or more morpholinophosphoramidate linkages resulted in reduced hybridization affinity relative to an unmodified DNA/RNA heteroduplex. Notably, when siRNA duplexes containing one or two terminal morpholinophosphoramidate linkages (3'- and 5'- ends) were treated with serum, their stabilities improved 4 to 7-fold relative to unmodified oligonucleotides. Improved serum stability has also been observed with other phosphoramidate analogues.[23-24] Of particular interest was the observation that siRNA duplexes containing morpholino phosphoramidate subunits were active at nanomolar concentrations in a dual luciferase reporter assay.

From a chemical perspective, the solid-phase synthesis of morpholinophosphoramidate ONs resulted in poor overall yields. Their crude reaction mixtures could not be purified using the conventional DMT-On/Off procedure due to their inherent instability to aqueous acid.[25] We hypothesized that replacing a non-bridging P=O linkages in morpholino phosphoramidates with P=S might reasonably improve their hydrolytic stability under acidic conditions and also increase their nuclease resistance towards intracellular enzymes. This rationale has led us to focus entirely on ONs containing thiophosphoramidate morpholinos (TMO, Figure 1c) and TMO chimeras containing DNA-pS linkages (Figure 1d). In this article, we evaluate the stability of TMO analogues towards aqueous acid, their hybridization affinity towards complementary DNA and RNA as well as their ability to recruit RNase H1. We further assess their biological potency as microRNA-15b inhibitors using a dual-luciferase reporter assay.

Results and Discussion

Chemical Synthesis

Morpholino nucleosides of N^6-benzoyl adenosine (mA^{Bz}), N^4-benzoyl cytidine (mC^{Bz}), N^2-isobutyryl guanosine (mG^{iBu}) and thymidine (mT) (compounds 3a-d) were synthesized according to published literature protocols (Scheme 1).[21-22,26] Briefly, 7.42 mmol of 5'-dimethoxytrityl (DMT) protected ribonucleoside (5.0 g (2a), 4.87 g (2b), 4.82 g (2c) or 4.16 g (2d)), was dissolved in 500 mL of anhydrous methanol followed by the sequential addition of 1.2 equiv. of sodium periodate (1.9 g, 8.9 mmol) and 1.2 equiv. of ammoniumbiborate tetrahydrate (2.35 g, 8.9 mmol). The mixture was stirred at 25 °C for 6 h or until no unreacted ribonucleoside could be detected by TLC. The reaction mixture was filtered through a pad of Celite®, and to the filtrate was added 2 equiv. of sodium cyanoborohydride (0.93 g, 14.8 mmol) and 2 equiv. of glacial acetic acid (0.85 mL, 14.8 mmol). The reaction mixture was stirred for 16 h, filtered, and the solvent was removed using a rotary evaporator. The crude reaction mixture was purified by chromatography on a silica gel column pre-equilibrated with ethylacetate (EtOAc) containing 3% triethylamine. The column was first eluted with 100% EtOAc followed by EtOAc:Methanol (70:30) to yield the 6'-DMT[27] protected morpholino nucleosides (3a-d): mA^{Bz} (2.75 g, 56%), mG^{iBu} (2.21 g, 46%), mC^{Bz} (2.40 g, 51%) and mT (2.33 g, 58%).

Zhang et al. have reported the chemical synthesis of morpholino phosphorodiamidites of mU and mT.[21-22] Following slight modifications to these protocols, phosphorodiamidites of mA^{Bz}, mG^{iBu}, mC^{Bz} and mT (4a-d, Scheme 1) were synthesized.[26] Briefly, one equivalent of each morpholino nucleoside (2.6–3.1 g, 4.8 mmol) and 1.2 equivalents of 2-cyanoethyl *N*,*N*,*N*',*N*'-tetraisopropyl phosphorodiamidite (1.83 mL) was reacted with 0.5 equivalents of 0.25M 5-(Ethylthio)-1*H*-tetrazole (ETT, 9.6 mL) in dichloromethane for 30 minutes. After evaporating to dryness, the crude product was quickly purified by column chromatography. The pure phosphorodiamidites were isolated in moderate yields (4a: 2.75 g, 67%, 4b: 2.37 g, 59%, 4c: 2.63 g, 66%, and 4d: 2.93 g, 82%). The detailed synthetic protocol and characterization data (^{1}H, ^{31}P, ^{13}C, ESI-MS) for all morpholino phosphorodiamidites are provided in the Supporting Information (SI, Section 2 and SI p.S45-S48).

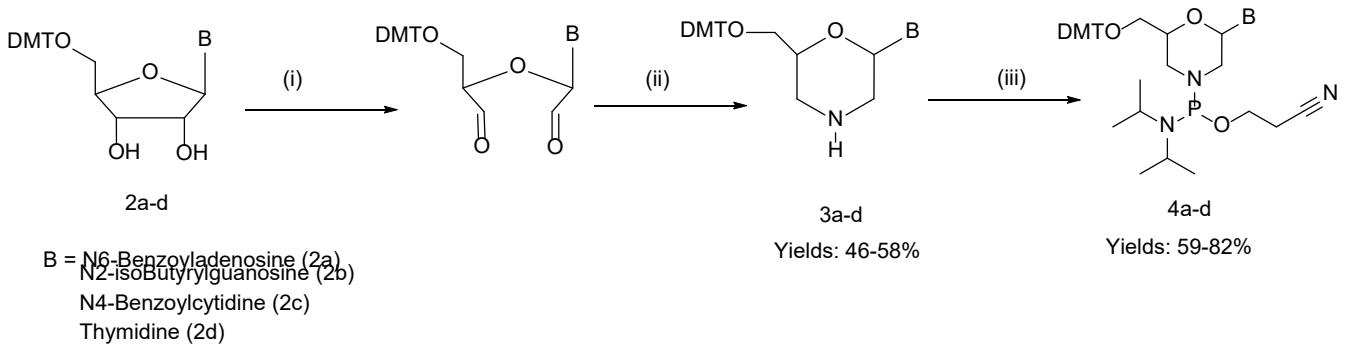

Scheme 1 Chemical synthesis of phosphorodiamidite synthons 4a-d. Reagents and conditions: (i) $NaIO_4$ (1.2 equiv.), anhydrous methanol; $(NH_4)_2B_2O_7$ (1.2 equiv.), 6 h (ii) $NaCNBH_3$ (2.0 equiv);CH_3COOH (2.0 equiv.), 16h (iii) $(OCH_2CH_2CN)P[N(iPr)_2]_2$ (1.2 equiv.), 5-Ethylthio-1*H*-Tetrazole (0.5 equiv.),CH_2Cl_2, 30 min.

Optimization of TMO Synthesis

Unlike conventional nucleoside phosphoramidites of the general formula $(R_1O)(R_2O)P[(N,N'\text{-}(iPr)_2]$ (Figure 2, **A**), where only one P(III)-N linkage is activated during the coupling step,[28] phosphorodiamidite morpholino synthons (4a-d) contain two P(III)-N linkages (Figure 2, **B**) both of which can get activated to different degrees depending upon the reaction conditions. Barone et al. demonstrated that when a phosphorodiamidite comprising two amino substituents, i.e., *P*-Methoxy-(*N,N'*-diisopropylamino,*N*-morpholino) phosphorodiamidite, was reacted with 1*H*-tetrazole, activation of the *N,N'*-diisopropylamino group was the major pathway, leading to the formation of morpholino substituted *P*-Methoxy phosphoramidite as the major product (95%), with only 5% of morpholino activated product.[29a] Since protonation of the amine leaving group and weakening of the P-N bond is the first step during phosphoramidite activation, the more basic diisopropylamino group (pKa = 11.07, water) has a greater propensity for protonation compared to the morpholino ring nitrogen (pKa = 8.49, water), making it a superior leaving group. Thus, previous studies comparing 1*H*-tetrazole-mediated activation of 5'-DMT-2'-deoxythymidine phosphoramidites containing either *N*-morpholino or *N,N'*-diisopropylamino as the amine leaving group showed 95% activation of the diisopropylamino group within 1 minute, whereas only 5 % activation of the morpholino group was observed under the same conditions,[29b] suggesting that the morpholino ring nitrogen might be less susceptible to activation when compared to the *N,N'*-diisopropylamino group.

Previous studies have shown that the specificity of activation of the morpholino ring nitrogen versus the *N,N'*-diisopropylamino group was dependent on the activator. When 0.5 equivalents of ammonium tetrazolide salt was used to activate *P*-Methoxy-(*N,N'*-diisopropylamino,*N*-morpholino) phosphorodiamidite, 10% of morpholino activated product was observed[29a] as opposed to only 5% morpholino activated product while using 1H tetrazole.[29b] In line with this observation, our preliminary attempts to synthesize TMOs using 0.45 M 1*H*-tetrazole or 0.25 M ETT resulted in poor overall yields and the concomitant formation of large amounts of side products.

To summarize, the lack of highly selective activation of the *N,N'*-diisopropylamino group versus the 6'-DMT-morpholinonucleoside can lead to an exponential loss of yields during the synthesis of mixmer TMOs for biological applications (≥ 25 mers). Therefore, an important step during coupling optimization was to determine which activator generated the highest yield of final product while minimizing the amount of truncated failures and associated side products.

In order to address this problem, several dodecathymidylate TMOs were synthesized under identical conditions except that different activators were used during the coupling step. Since the poor yields could be mainly due to competing activation of the 6'-DMT-morpholino subunit, all activators were tested at 50% of their manufacturer recommended concentrations. We anticipated that an increased coupling time of 600 seconds might compensate for any loss of reactivity owing to the lower activator concentrations. Post synthesis, the ratio of full-length product versus failures in the total reaction mixture was calculated by integrating their UV profiles. The ratio of the expected product (TMO1, Table 1) in each case is shown in SI Figure S1.

During TMO synthesis, the coupling step must proceed by protonation of the phosphorodiamidite followed by displacement of one of the amine leaving groups resulting in a reactive intermediate which further undergoes nucleophilic attack.[30] We first investigated the effect of high acidity (faster protonation rate) on amine selectivity. The lowest yields (61.7%) were obtained for the highly acidic 5-[3,5-bis(trifluoromethyl)phenyl]-1*H*-tetrazole (Activator 42®, pKa = 3.4) (SI Figure S1a). This could be the result of competing morpholino activation leading to premature self-capping of the growing TMO chain as a 5'-*N,N'*-diisopropyl phosphoramidate. Additionally, 6'-DMT detritylation, stepwise double activation of the incoming phosphorodiamidite or degradation of the TMO backbone due to the high acidity of Activator 42® may occur during the long coupling step (600s wait).

Low yields (65.6%) and large amounts of failure products were also observed when 0.12 M 1*H*-tetrazole (TET, pKa = 4.9) was used. The presence of a significant amount of very

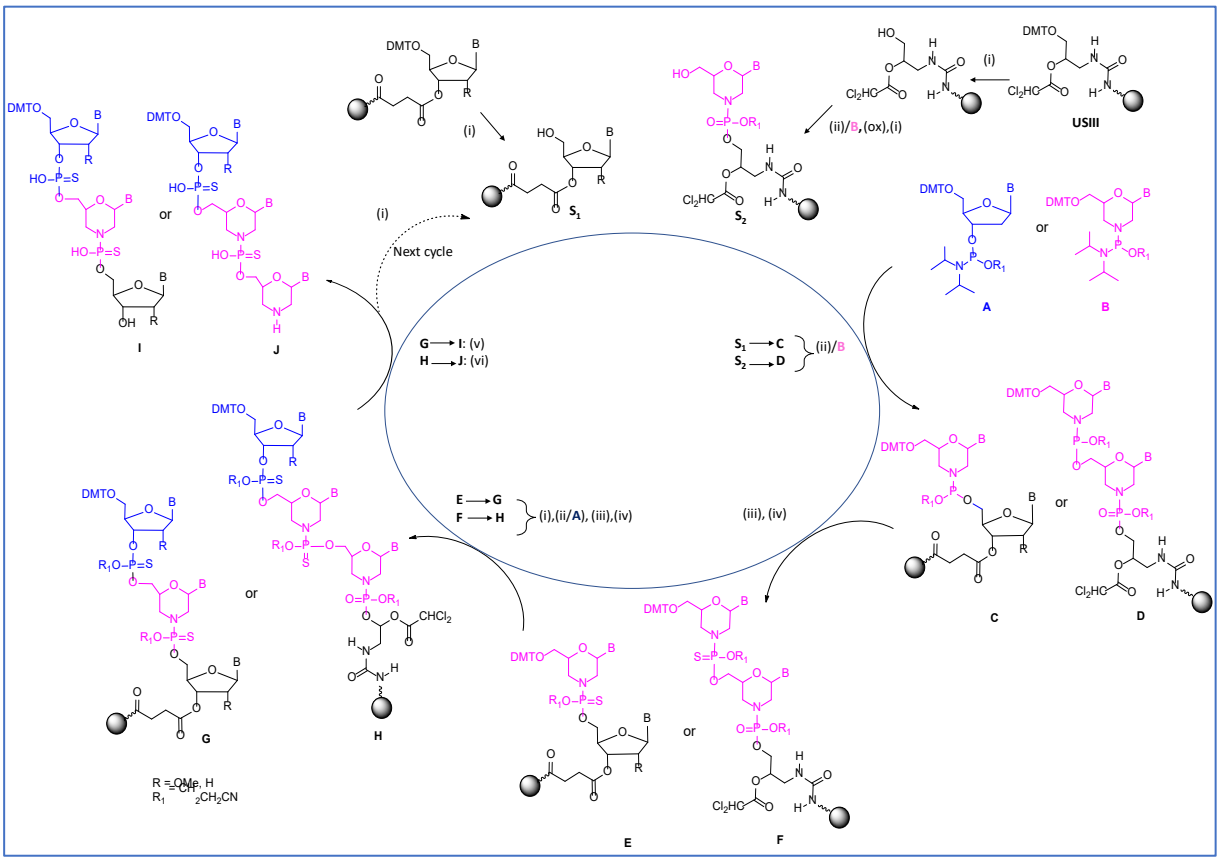

Figure 2 Solid-phase Synthesis of TMO and TMO-DNA-pS Chimeras; Reagents: (i) Detritylation: 3% trichloroacetic acid/CH_2Cl_2 (ii) Condensation: 0.12M 5-Ethylthio-1H-tetrazole/CH_3CN, 600s wait (iii) Sulfurization: 0.05 M DDTT/pyridine/CH_3CN (iv) Capping: Ac_2O/pyridine/THF; 1-Methylimidazole/CH_3CN (v) Deprotection: 28% aqueous ammonia, 55 ^oC, 16 h or (vi) Deprotection: 2M ammonia in methanol, 60 min, followed by 28 % aqueous ammonia, 55 ^oC, 16 h. Amidites A, B are color-coded to simplify the cycle.

short failure products (Rt = 1.5–7 min; SI Figure S1c) suggests the lower stepwise coupling efficiency of TET. Since 5-Ethylthio-1*H*-Tetrazole is more acidic than 1*H*-tetrazole (ETT, pKa = 4.3), the following conditions were tested: 0.12 M ETT buffered with 0.01M DMAP[31] (SI Figure S1b) and 0.12 M ETT (SI Figure S1e). Surprisingly, the highest yield of full-length product was obtained for unbuffered, 0.12 M ETT (85.9%). The less acidic, more nucleophilic 4,5-dicyanoimidazole (DCI, pKa = 5.2) also produced TMO1 in relatively high yields (0.12 M DCI, 82.3%; SI Figure S1d). Attempts to increase the nucleophilicity by using DMAP-buffered ETT produced the expected product in lower yields compared to unbuffered ETT (SI Figure S1b, 79.6%). These observations suggest that apart from activator pKa, several other parameters such as nucleophilicity, coupling time and activator concentration play a major role in determining stepwise yields during TMO synthesis. Based on the above results, 0.12 M ETT was chosen as the activator of choice for solid-phase synthesis.

To elucidate the role of activator concentration (0.25–1.5 equiv.) on product selectivity, the solution-phase reactivity of 6'-DMT-morpholinothymidine phosphorodiamidite (4d, Scheme1) with 3'-O-acetyl thymidine was monitored using ^{31}P NMR as described elsewhere.[25] While lower ETT concentrations (0.25 equiv.) resulted in sluggish reactions and higher percentage of morpholino activation, using 1.0 equiv. or more of ETT resulted in step-wise activation of both amino substituents and produced symmetrical dithymidine phosphotriester in significant amounts.

In summary, the solid-phase synthesis of TMOs and their chimeras (Figure 2) reported here closely follows conventional phosphorothioate DNA synthesis with only two differences: (i) ETT concentration was reduced to 0.12 M instead of the manufacturer recommended 0.25 M (ii) a 600 s coupling time was used. For synthesizing TMO-DNA-pS chimeras, a 30 second coupling time was used for commercially obtained 2'-deoxyribonucleotide 3'-phosphoramidites. The detailed solid-phase synthesis protocol is summarized in the SI, Section 3.

Optimization of DMT-On/Off Purification

Previous studies on the kinetic and mechanistic aspects of hydrolysis of 3',5'-thiophosphoramidates under a wide pH range (pH 1-9) have shown that protonation of the 3'-nitrogen generates a N(H)-P(V) linkage which is susceptible to degradation at low pH (pH < 5).[32-33] Since TMO subunits contain a P(V)-(*N*-morpholino) linkage, we evaluated the hydrolytic stability of TMO1 (Table 1) under acidic pH. TMO1 (Table 1) was treated with various concentrations of aqueous acetic acid and the rate of degradation over time

Table 1. List of Oligonucleotides and Their Respective Yields**

ON#	Sequence Design*	Yields nmoles (μg)	Theoretical Mass	Observed Mass‡
1	6'-DMT-TTT TTT TTT TTt-3'	275.9 (990.6)	4053.6519	4053.659
2	6'-DMT-AGT TGC CCT GTG dT^{Fl} -3'	138.0 (682.9)	4948.8879	4948.897
3	6'-T GTA AAC CAT GAT GTG CTG CTa-3'	46.8 (315.8)	7061.0162	7061.029
4	6'-T GTA aac cat gat gtg ctG CTa-3'	117.0 (789.5)	7074.7924	7074.806
5	5'-tGtA aAc CaT gAt GtG cTg Cta-3'	88.9 (600.0)	7071.8403	7071.854
6	6'-T gTaA aCc AtG aTg TgC tGc Tat-3'	117.0 (789.5)	7390.8795	7390.894
7	6'-Fl$_s$-TT TTT TTT TTT TTt-3'	202.7 (1021.4)	4942.6956	4942.704
8	6'-Fl$_s$-TT TTT TTT TTT TTT-3'	181.7 (915.7)	4941.7116	4941.721
9	6'-ATC CAA CTT ACC GTG ATc-3'	164.1 (888.7)	5670.8291	5670.839
10	5'-Fl$_s$-t$_p$t$_p$t$_p$ t$_p$t$_p$t$_p$ t$_p$t$_p$t$_p$ t$_p$t$_p$t$_p$ t$_p$tT-3'	622.1 (3134.6)	5066.8240	5066.819
11	5'-Fl$_s$-t$_p$t$_p$t$_p$ t$_p$t$_p$t$_p$ t$_p$t$_p$t$_p$ t$_p$t$_p$t$_p$ t$_p$t$_p$T-3'	650.1 (3275.5)	5050.8468	5050.843
12	5'-Fl$_s$-ttt ttt ttt ttt tt -3'	807.7 (3823.7)	–	–
13	5'-Fl$_s$-t$_p$t$_p$ t$_p$t$_p$t$_p$ t$_p$t$_p$t$_p$ t$_p$t$_p$t$_p$ t$_p$t$_p$t-3'	829.9 (3929.0)	–	–
14	6'-ATA AAC AGA GGG ATT TAC Ca-3'	70.4(433.7)	6439.9657	6439.978
15	6'-GAG TCA TTC GAC TTC TGA Ct-3'	155.4 (946.0)	6364.9085	6364.921
16	6'-ATG ATG AGC TAC TGT ATC GCTa-3'	151.8 (1023.7)	7061.0162	7061.030

** Uppercase, underline: TMO; lowercase: 2'-deoxynucleotide pS; lowercase with subscript p: 2'-deoxynucleotide phosphate; Fl$_s$: Fluorescein pS. *Unless specified with subscript p (phosphates), all internucleotide linkages are phosphorothioate (pS) or thiophosphoramidate. ‡For HRMS data of TMOs, please see SI, p.S49-S62. For percentage yields (DMT-ON), see SI Table S1, p. S21.

was monitored by LCMS. Under the conditions used for conventional DMT-On/Off purification[34] (80% aqueous acetic acid), TMO1 was completely degraded within 10 min at 25 °C (data not shown). Therefore, the acid concentration was reduced to 50%. The rate of degradation of TMO1 over time under this condition is shown in SI Figures S15a-e. We determined that a 5 min treatment with 50% aqueous acetic acid followed by immediate quenching with triethylamine resulted in > 99% detritylation of TMO1 (SI Figure S15b) with minimal degradation, making this our preferred method for DMT deprotection (See SI Section 3 for details). Using this protocol, the final DMT-Off oligonucleotides were > 85 % pure on average as determined by LCMS.

Following this procedure, several TMO mixmer ONs and chimeric TMO-DNA-pS ONs were synthesized and their LCMS characterization data is provided in Table1. Where applicable, the percentage yields of full-length DMT-ON product versus failures were obtained by integrating the UV profiles of LCMS data and is provided in SI Table S1, p.21. In order to further establish proof-of-concept for the robust synthesis of TMOs using the solid-phase synthesis procedure as outlined in Scheme 2, the spectra of crude, unpurified reaction mixtures for TMOs 14-16 are shown in the SI Figures S12(a), S13, and S14. Integration of UV profiles of mixmer ONs revealed that the 6'-DMT ON product was obtained in 30-45% yield (SI Table S1). We noted that apart from % GC content and ON length, the purity and moisture content of morpholino phosphorodiamidites play a vital role in obtaining satisfactory yields. Thus, the average stepwise yields varied from 95-97% per coupling (ABI-394, trityl monitoring). After DMT-On/Off purification, the TMO oligonucleotides were obtained in moderate yields (47-276 nanomoles, Table 1). Comparable yields were also obtained for TMO-DNA-pS chimeras (ONs 4, 5, 6; Table 1 and SI Figures S4-S6).

For purposes of yield comparison, 14-mer DNA-pS ON12 and unmodified DNA ON13 produced > 800 nmoles of pure product under the newly optimized TMO synthesis conditions. TMOs 8, 10, and 11 with a 3'-morpholino moiety were synthesized using Universal Support III (Glen Research, VA). In this case, the first morpholino phosphorodiamidite coupling step was followed by oxidation instead of sulfurization (USIII to S2, Figure 2). All subsequent synthesis steps were identical while using either solid support. Oligonucleotide cleavage from USIII support was carried out using 2M ammonia in methanol for 1 h followed by deprotection using 28% aqueous ammonia at 55 °C for 16 h.

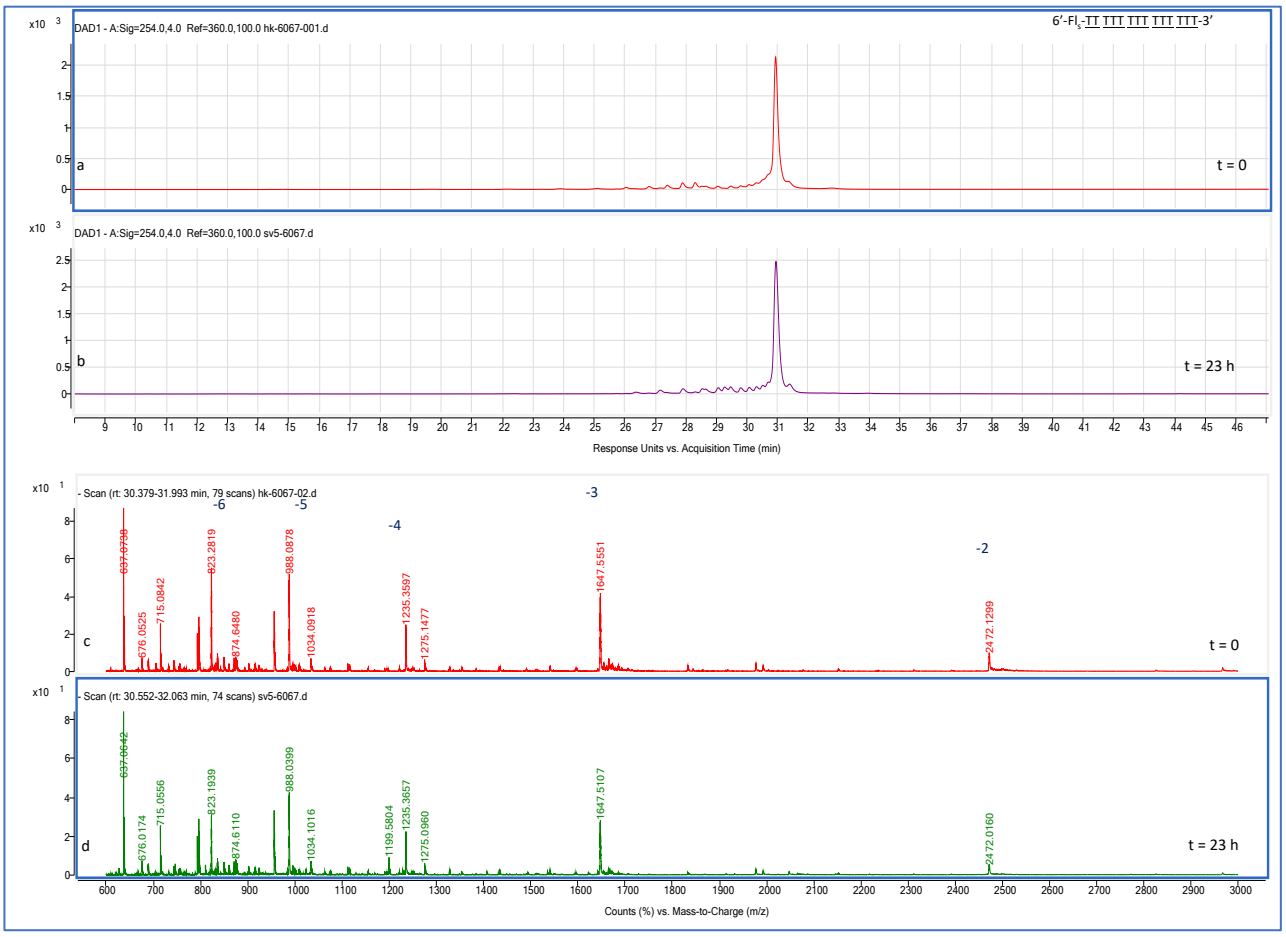

Figure 3 LCMS Analysis of TMO8 During the SVPDE Assay. Analytical RP-HPLC Fractions corresponding to TMO8 were collected at various time points during SVPDE treatment (SI Figures S18-S23: Collected fractions with Rt = 13-16 min). Figure 3(a, b) show the LCMS UV profiles corresponding to TMO8 after SVPDE treatment (t = 0, 23 h). Figure 3(c, d) compare the m/z data at t=0 (untreated) and t =23 h.

Enzymatic Stability

While phosphorothioate ONs are more stable towards enzymatic degradation when compared to unmodified DNA,[35] no enzyme is known to degrade non-ionic PMOs.[36] Since TMOs are hybrid molecules containing both morpholino nucleosides and pS linkages, we hypothesized that they might possess superior enzymatic stability to nucleases relative to unmodified DNA.

The 3'-exonuclease susceptibility of exclusively thiophosphoramidate modified TMO8 and DNA-pS control ON12 (Table 1) were evaluated using Snake Venom Phosphodiesterase I (SVPDE). While performing enzymatic hydrolysis experiments, TMO8 and ON12 (13.3 μM) were incubated at 37 °C in a reaction mixture containing 100 mM Tris-HCl buffer (pH 8.5), 14 mM $MgCl_2$, 72 mM NaCl and SVPDE enzyme (0.1 U/ mL). Aliquots (45 μL) were withdrawn at various time points, heat inactivated and stored in dry ice until analyzed by analytical RP-HPLC.

Based on analytical RP-HPLC analysis (SI, Figures S18-S23), no detectable degradation or peak broadening was observed for TMO8 over a period of 23 h. The undegraded TMO8, with a Rt = 13-16 min, is the major product (two minor products at 11 and 11.8 min could be degradation products but the remaining minor peaks are from the enzyme as shown in Figure S16). When subjected to the same assay conditions, considerable peak broadening was observed for ON12 within 7 h (SI Figures S26- S29). Additionally, the appearance of a fast eluting peak (Rt = 1.5 min, Figure S29), presumably arising from 5'-pS-thymidine mononucleotide, was also observed during this time frame.

Undegraded TMO8 and its potential enzymatic degradation products (n-1, n-2 etc.) might co-elute on a reverse-phase C18 column during analytical RP-HPLC. To address this, the peaks observed at each time point during the SVPDE assay was collected, pooled and reanalyzed by LCMS. In case of TMO8, the analytical HPLC fractions corresponding to the UV signal at Rt = 13-16 min at various time points during the SVPDE assay (SI, Figures S18-S23: time points 1, 4, 8, and 23 h) were re-analyzed by LCMS (Figure 3 a, b and SI Figure S24). By comparing these reanalysis profiles with that of untreated TMO8 and analyzing their corresponding m/z data (Figure 3c, d: t = 0 and 23 h), we confirmed that TMO8 did not degrade within 23 h during our SVPDE assay conditions. We therefore concluded that in comparison to DNA-pS ONs, TMOs are highly stable towards Snake Venom Phosphodiesterase I.

The SVPDE assays for DNA-pS ON12 and unmodified phosphate DNA (ON13) was performed using the same protocol as described for TMO8. The fractions corresponding to the broad peak at Rt = 14–16 min (Analytical RP-HPLC profiles in SI Figures S26-S29) were re-analyzed by LCMS (SI Figure S30). Although accurate quantification of each degradation product could not be obtained due to partially overlapping signals, the LCMS analysis of ON12 at t =7 h after SVPDE treatment showed that essentially complete degradation had occurred. In comparison, unmodified DNA ON13 was completely degraded within 15 minutes under these conditions (SI Figure S31).

We routinely employ 1.0 μM succinyl CPG loaded with 2'-deoxynucleosides or 2'-OMe nucleosides in order to generate TMOs (e.g., all ONs in Table 1 except 8, 10 and 11). Therefore, the 3'-exonuclease susceptibility of TMO7 (Table 1) containing a 2'-deoxythymidine moiety as the 3'-unit was also evaluated using the above method (100 mM Tris pH 9, 14 mM $MgCl_2$, 72 mM NaCl, 13.3 μM TMO7, $2x10^{-1}$ U/mL SVPDE enzyme, 37 °C). As expected, no degradation of TMO7 was observed over a period of 23 h (confirmed by LCMS re-analysis, SI Figure S32).

Thermal Denaturation Studies

The binding affinity of an oligonucleotide plays a critical role in shaping its therapeutic potential. Since the advent of LNA,[37] several conformationally locked sugar modifications have been developed to improve the binding affinity of ONs.[38] Among unnatural backbone constructs, PMOs and PNAs improve RNA hybridization affinity[39-40] whereas stereorandom ONs consisting of phosphorothioates[41] and boranophosphates[42] decrease binding affinity. Although phosphoramidate ONs[23] and chimeric morpholino phosphoramidate-DNA have exhibited decreased RNA binding affinity,[21] N3'-P5' phosphoramidates and their thiophosphoramidate variants as well as triazole-linked morpholino oligonucleotides[20] have been shown to form highly stable duplexes with RNA.[43]

Encouraged by the increased RNA binding affinity of various morpholino and thiophosphoramidate analogues, the hybridization affinity of TMO and TMO-DNA-pS chimeras 3–6 (Table 1) towards complementary DNA and RNA were investigated. Control duplexes of the same sequence consisting of PMO, DNA-pS or canonical DNA were also evaluated under identical conditions. Briefly, ONs 3-6 and their DNA or RNA complements (1.0 μM in each strand) were dissolved in a suitable buffer (50 mM Tris-HCl, 50 mM KCl and 1 mM $MgCl_2$, pH 8.3). DNA and RNA duplexes of PMO, DNA-pS, canonical DNA were also prepared under identical conditions and used as controls. Each duplex (total volume =1.0 mL) was added to a 10 mm path length cuvette and placed in a 6x6 Peltier thermostatted multi-cell holder. The samples were heated from 15–90 °C at a 3 °C/min ramp rate, maintained at 90 °C for 5 min and cooled to 10 °C at a 1 °C/min ramp rate before initiating thermal runs (0.5 °C/min ramp rate). Each experiment was repeated at least two times per duplex (4 curves). Representative thermal runs for all duplexes are provided in SI Section 6, Figure S33, pp. S39–S41.

When compared to the canonical DNA/DNA duplex, the TMO3/DNA duplex showed a depression of -12.6 °C (- 0.6 °C per TMO modification). This loss of binding affinity is greater than that for the DNA-pS/DNA duplex (Tm depression of 8.2 °C; -0.4 °C per modification). In comparison, fluorescently labeled Fl-PMO/DNA exhibited a Tm close to the native DNA/DNA duplex with a loss of only 1.5 °C – a reduction that could be attributed to the presence of a 3'-fluorescein label on the PMO. TMO-DNA-pS chimera 4 (32% TMO modified with a gapmer[37] configuration, 7 TMO linkages, Table 1), exhibited a depression of -6.6 °C (-0.9 °C per TMO modification). Surprisingly, TMOs 5 and 6 which are composed of alternating TMO and DNA-pS linkages presented an increase in Tm by ~ +6.5 °C (+0.6 °C per TMO modification) when duplexed with complementary DNA. To summarize, Tm values for ON/DNA duplexes of ONs 3-6 displayed the trend: TMO5/DNA ~ TMO6/DNA> DNA/DNA ~ Fl-PMO/DNA > TMO4/DNA > DNA-pS/DNA > TMO3/DNA.

Contrary to its DNA duplex, the TMO3/RNA duplex showed an increase in Tm by +10 °C (+0.48 °C /TMO linkage) when compared to the unmodified DNA/RNA duplex. Similarly, Fl-PMO/RNA duplex also showed a Tm increase of +0.4 °C per modification. TMO5 and TMO6 which contain alternating morpholino thiophosphoramidate and DNA-pS linkages showed a Tm increase ≥ +9.6 °C (+0.88 – 1°C /TMO linkage), which is the highest Tm increase observed for any duplex discussed in this work.

The DNA-pS/RNA control duplex showed a -0.4 °C depression per DNA-pS linkage as expected,[44] and the gapmer TMO4/RNA duplex showed a depression of -0.5 °C per TMO linkage. This may be attributed to the nature of the gapmer design (small TMO 'wings' and a 14-mer DNA-pS 'gap'). Thus, the RNA duplexes of TMOs 3-6 followed the trend: TMO5/RNA ~ TMO3/RNA ~ TMO6/RNA > Fl-PMO/RNA > DNA/RNA > TMO4/RNA > DNA-pS/RNA.

To summarize, alternately modified TMO5 and TMO6 showed an increase in binding affinity (+6–10 °C) towards both complementary DNA and RNA. We hypothesize that the insertion of alternating 2'-deoxynucleotides after each TMO subunit might provide increased flexibility to an otherwise rigid construct, permitting more efficient binding with the complementary strand.

A significant loss T_m (>12 °C) was observed for the TMO3/DNA duplex. Similarly, Fl-PMO also did not show increased binding affinity towards complementary DNA, suggesting that the exclusive presence of rigid morpholino moieties results in a backbone conformation that is not conducive to efficient DNA binding. The DNA-pS/DNA duplex also showed a reduced T_m (-8.2 °C), as expected. Thus, it can be hypothesized that the TMO3 construct, being a perfect hybrid of both rigid morpholino sugars and pS internucleotide linkages, suffers a cumulative loss of DNA binding ability. In contrast, both TMO3 and Fl-PMO showed superior RNA binding affinity (+8–10 °C).

Table 2. T_m data of DNA and RNA duplexes of TMOs 3-6

Duplex*	Sequence Design[#,‡]	TMO Mod	Tm	ΔTm	ΔTm/ mod[¶]	SD
DNA/DNA	5′-t$_p$ g$_p$t$_p$a$_p$ a$_p$a$_p$c$_p$ c$_p$a$_p$t$_p$ g$_p$a$_p$t$_p$ g$_p$t$_p$g$_p$ c$_p$t$_p$g$_p$ c$_p$t$_p$a-3′	0	64.82	–	–	0.4
DNA-pS/DNA	5′-t gta aac cat gat gtg ctg cta-3′	0	56.60	-8.22	-0.40	0.3
TMO3/DNA	6′-T GTA AAC CAT GAT GTG CTG CTa-3′	21	52.20	-12.63	-0.60	1.5
TMO4/DNA	6′-T GTA aac cat gat gtg ctG CTa-3′	7	58.21	-6.61	-0.90	0.6
TMO5/DNA	5′-tGtA aAc CaT gAt GtG cTg Cta-3′	10	71.41	6.59	0.66	0.9
TMO6/DNA	6′-T gTaA aCc AtG aTg TgC tGc Tat-3′	11	71.77	6.95	0.63	0.5
Fl-PMO/DNA	6′-*t gta aac cat gat gtg ctg cta*-Fl-3′	0	63.32	-1.50	0.0	0.7
DNA/RNA	5′-t$_p$ g$_p$t$_p$a$_p$ a$_p$a$_p$c$_p$ c$_p$a$_p$t$_p$ g$_p$a$_p$t$_p$ g$_p$t$_p$g$_p$ c$_p$t$_p$g$_p$ c$_p$t$_p$a-3′	0	64.45	–	–	0.1
DNA-pS/RNA	5′-t gta aac cat gat gtg ctg cta-3′	0	56.20	-8.25	-0.40	0.4
TMO3/RNA	6′-T GTA AAC CAT GAT GTG CTG CTa-3′	21	74.43	9.98	0.48	0.2
TMO4/RNA	6′-T GTA aac cat gat gtg ctG CTa-3′	7	60.68	-3.77	-0.54	0.4
TMO5/RNA	5′-tGtA aAc CaT gAt GtG cTg Cta-3′	10	74.50	10.05	1.00	0.9
TMO6/RNA	6′-T gTaA aCc AtG aTg TgC tGc Tat-3′	11	74.10	9.65	0.88	0.7
Fl-PMO/RNA	6′-*t gta aac cat gat gtg ctg cta*-Fl-3′	0	72.65	8.19	0.40	0.6

*Canonical DNA, Fl-PMO and DNA-pS duplexes were utilized as controls. # Complementary strands were unmodified DNA or RNA; ‡Uppercase, underline: TMO; lowercase: 2′-deoxynucleotide pS; lowercase, subscript p: 2′-deoxynucleotide phosphate; lowercase, italics: PMO; Fl: Fluorescein. ¶ no TMO modifications are present in Fl-PMO: Tm/mod was calculated based on Tm difference w.r.t the corresponding DNA/DNA or DNA/RNA control duplex. SD: standard deviation.

Apart from the percent modification, the position of TMO linkages within the sequence appears to play a crucial role in determining its binding affinity. This becomes obvious while comparing the T_m values of TMO5, TMO6 (50% TMO modified) and gapmer TMO4 (32% TMO modified). When complexed to complementary RNA or DNA, the binding affinity of the latter was lower by ~ 14 ^oC.

Circular Dichroism Spectra

The conformation of canonical DNA/RNA heteroduplexes lies between A and B form helical geometries.[45] While both A and B form duplexes have maxima and minima at similar wavelengths, greater ellipticities between 270 nm and 280 nm is observed in the A-form, whereas a B-form duplex has approximately equal positive and negative bands above 220 nm with a crossover at 261 nm.[46] To gain additional insights into their global helical structure, RNA heteroduplexes of TMOs 3, 5 and 14 were assessed using circular dichroism and compared with control duplexes (DNA-pS/RNA, canonical DNA/RNA). Since the relative position and intensities of characteristic negative bands at 210 nm and the positive band around 280 nm for DNA/RNA hybrids are highly sequence dependent,[47] TMOs 3-6 and a DNA-pS control of identical sequence were used during this experiment, with the exception of TMO14 (Table 1).

As seen in Figure 4, the CD spectra of RNA duplexes of TMOs 3, 5 and 14 display the characteristic features of an A-type helical environment with negative bands of varying intensity ~210 nm and a positive band of strong intensity ~270 nm.[48] The positive Cotton band and the negative band at 210 nm characteristic of an A-form helical structure is most prominent in the TMO5/RNA heteroduplex, and closely resembles a typical A-form RNA/RNA duplex shown in SI Figure S34.[49] This observation further supports the hypothesis that the increased conformational flexibility gained by inserting 2′-deoxynucleotide linkages between TMO subunits imposes a more pronounced A-form conformation in its duplexes resulting in superior binding affinity for this design.

Crossover bands between 205 to 215 nm and 227 to 233 nm were observed for all duplexes except DNA-pS/RNA, which showed no crossover in these regions. The positive absorption band at 273 nm for the canonical DNA/RNA duplex (crossover at 257 nm) was blue shifted to ~265 nm for all TMO duplexes as well as the DNA-pS/RNA duplex (crossover wavelengths between 250-255 nm). Apart from the TMO5/RNA duplex, the gapmer TMO4/RNA duplex and the DNA-pS/RNA duplex also exhibits an intense negative peak in the 200-213 nm range which is characteristic of an A-form duplex.[48] In case of TMO14, this negative peak closely resembles that of canonical DNA/RNA control duplex (both duplexes crossover at 203, 211 nm). However, a lesser intense negative peak was observed for TMO3/RNA duplex which highlights the sequence dependence effects observed in CD spectra. In summary, the CD spectra of

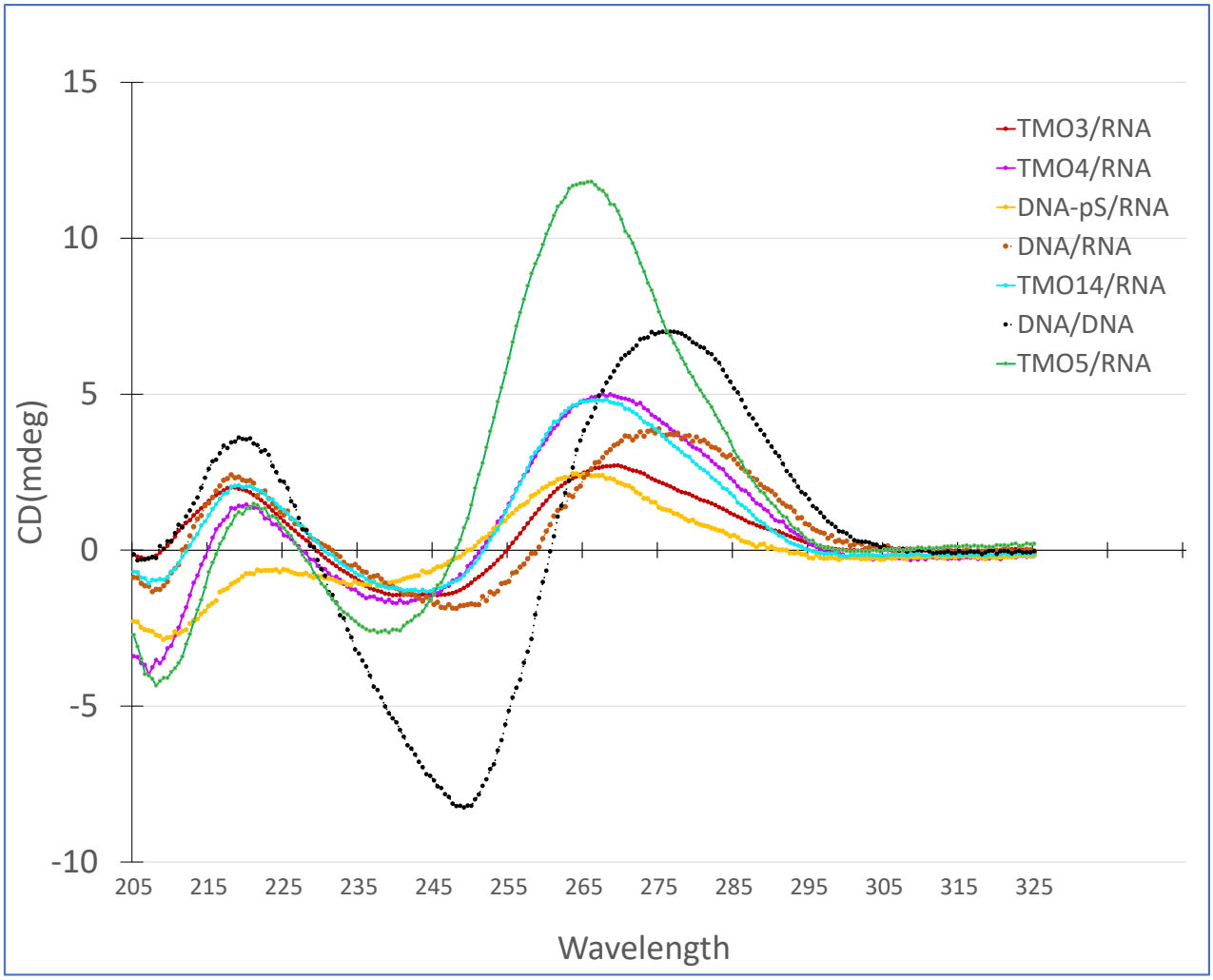

Figure 4 Circular Dichroism of TMOs 3, 4, 5 and 14 relative to DNA-pS/RNA, DNA/RNA and DNA/DNA as controls. An example for an A-form RNA/RNA control duplex is provided in SI Figure S34.

newly synthesized TMO heteroduplexes reveals its structural similarities to the DNA-pS/RNA duplex.[50] TMOs 3, 4 and 14 adopt helical conformations which are closer to an A-form rather than a B-form duplex. Interestingly, the uniformly TMO modified constructs (TMO3 and 14) yield RNA duplexes with notably different biophysical characteristics relative to chimeric TMO5. Thus, the TMO5/RNA duplex closely resembles an A-form RNA/RNA duplex, providing a logical explanation for its higher binding affinity towards complementary DNA and RNA. Further experiments designed to evaluate the helical conformations adopted by various TMO/DNA duplexes are currently underway.

RNase H1 Activity of TMO3/RNA and Gapmer TMO4/RNA Duplexes

RNase H enzymes constitute a large family of endonucleases that specifically digest the RNA strand which is hybridized to complementary DNA. These evolutionarily abundant, ancient enzymes are involved in numerous biological processes including degradation of RNA primers from Okazaki fragments during DNA replication, homologous recombination, DNA repair and RNAi.[51-52] Since retroviral reverse transcriptases (RT) contain an RNase H domain which is essential for reverse transcription of viral cDNA, the RNase H domain of HIV-RT is being evaluated as a potential target for the treatment of drug resistant HIV-1 strains.[53]

Antisense-based RNase H therapeutics gained substantial interest over four decades ago when Zamecnik et al. demonstrated that addition of short synthetic ONs (13-mers) targeting the viral repeat sequence of Rous sarcoma virus inhibited viral replication and oncogenic transformation of chicken fibroblast cells.[54] They successfully demonstrated the ability of ONs to inhibit gene expression by binding and then degrading the RNA target through the action of RNase H1.[55] Since this ground breaking work, several chemically synthesized oligonucleotide analogues have been evaluated for RNase H1 mediated antisense therapies. This is an attractive strategy since the reaction proceeds catalytically by releasing the ON drug for several successive rounds of RNA targeted inhibition. Examples of RNase H1 active chemical modifications include phosphorothioates,[56] boranophosphates[57], mesylphosphoramidates[58] and sugar

modifications such as arabinonucleic acid,[59] cyclohexene nucleic acid[60] and 2'-fluoro arabinonucleic acid.[61]

TMOs exhibit higher RNA binding affinity relative to canonical control duplexes, possibly allowing them to efficiently invade RNA secondary structures. They also possess superior enzymatic stability which makes them ideal candidates for RNase H1 based therapeutics. To evaluate this aspect, TMO3 was preannealed with a 5'-fluorescein labeled complementary RNA and digested with Escherichia coli RNase H1. The results were analyzed by PAGE (detailed experimental protocol in SI Section 7) and visualized using a transilluminator to detect the 5'-fluorescein tag attached to RNA (Lanes 1, 2; Figure 5). No degraded 5'-Fl-RNA fragments were observed in case of the TMO/RNA duplex after RNase H1 treatment. We therefore concluded that the TMO3/RNA duplex is not RNase H1 active.

It is well known that RNase H1 inactive ONs can be rendered RNase H1 active by adopting a gapmer ON design, where such modifications flank the RNase H1 active DNA or DNA-pS segment.[62] We therefore explored the RNase H1 activity of gapmer TMO4 containing TMO wings and a 14-mer DNA-pS gap. The experiment was carried out using the same protocol as described for TMO3. The results shown in Figure 5 (Lanes 3, 4) illustrate that TMO4 stimulates RNase H1 activity.

Further insights into the RNase H1 recruiting ability of certain chemical modifications versus those that are inactive can be gained from the crystal structure analyses of human RNase H1 complexed with several DNA/RNA duplexes, as described by Nowotny et al.[63] Although the RNA-binding domain of the enzyme directs positional preference for the cleavage site,[64] its catalytic core primarily interacts with the minor groove of an 11-bp RNA/DNA duplex segment. The RNA strand precisely fits into one of the two grooves present in the active site where it adopts a regular A-form structure and is largely recognized through interactions with four 2'- hydroxyl residues located around the scissile phosphorus within the catalytic core.

DNA modifications with high flexibility have been shown to ablate RNase H1 activity.[65] Nevertheless, the specificity of the DNA strand is imposed by a conformational flexibility requirement that permits its inclusion into the phosphate binding pocket. Since large distortions to the torsion angles of the ON backbone are required to position the DNA strand within this pocket, only a flexible B-form oligonucleotide can satisfy this requirement. Additionally, this strand must be able to precisely fit within the DNA-binding channel formed by the "basic protrusion" site. It is also required to undergo numerous physical distortions within this channel, resulting in a heteroduplex that is between A and B form. The specificity of DNA over RNA is further imposed by a steric requirement, i.e., the absence of 2'-hydroxyl groups, which in turn allows hydrogen bonding and van der Waals interactions within the basic protrusion channel. Thus, RNase H1 has highly complex structural requirements such that even a single chemical modification when appropriately positioned within a DNA strand can abolish RNase H1 activity at a previously characterized cleavage site.[65-66]

Based on these findings, we hypothesize that the lack of RNase H1 activity of the TMO3/RNA duplex might be due to its lack of conformational flexibility due to the presence of rigid, 6-membered morpholino rings throughout its backbone, which precludes it from entering the phosphate binding pocket or interacting effectively with the DNA binding channel within the enzyme's catalytic site. This hypothesis is further supported by the work of ∅stergaard et al;[66] they recently demonstrated that a fluorinated nucleoside modification containing a rigid six-membered ring (FHNA), when systematically walked through every position along the gap region of a 3-9-3 gapmer showed a marked decrease in RNase H1 activity at most positions when compared to its 2'-fluoro-2'-deoxynucleoside analog (FRNA).[66]

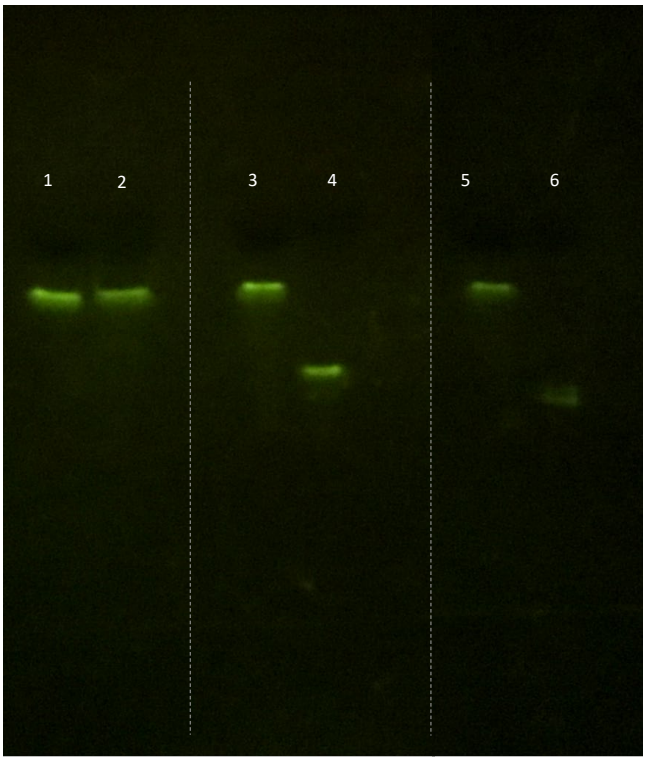

Figure 5 Gel electrophoresis images of 5'-Fl-RNA duplexes of TMOs 3, 4 and control DNA-pS following the E. Coli RNase H1 assay. Fluorescence arises only from intact 5'-Fl-RNA or its degraded fragments. Lane 1: TMO3/RNA duplex ctrl; Lane 2: TMO3/RNA duplex + RNase H1; Lane 3: TMO4/RNA duplex ctrl; Lane 4: TMO4/RNA duplex + RNase H1; Lane 5: DNA-pS/RNA duplex ctrl; Lane 6: DNA-pS/RNA duplex + RNase H1.

TMO4, on the other hand, encompasses a large 14 nucleotide DNA-pS gap, and is RNase H1 active. This can be explained based on previous work that a 7-10 nucleotide gap length was sufficient to allow for efficient RNase H1 catalysis[67] but a complete loss in activity occurs when the gap length was < 5 deoxynucleotides.[68] Additionally, comprehensive sequencing-based experiments that characterized the sequence preferences of various RNase H1 enzymes have shown that RNA cleavage sites predicted

to have the highest probability for RNase H1 cleavage falls within this gap length.[69]

In summary, exclusively TMO modified ONs (e.g., TMO3) do not elicit RNase H1, presumably due to their conformational rigidity. Nevertheless, a gapmer design such as TMO4 is rendered RNase H1 active. This suggests that exclusively TMO modified ONs are potential candidates for exon skipping experiments where they function as steric blockers, whereas gapmers having TMO wings can be used for antisense experiments that involve mRNA degradation through activation of the RNase H1 pathway.

Evaluation of TMOs as miRNA Inhibitors

MicroRNAs (miRNAs) are short non-coding RNAs that play major roles in post-transcriptional gene regulation by fine-tuning both the stability and rate of translation of mRNAs.[70] They suppress translation by guiding the miRISC complex to partially complementary sites in the 3'-UTR of their mRNA target, resulting in deadenylation, translational repression or mRNA degradation.[71] They have been widely implicated in the pathogenesis of various human diseases making them attractive targets for oligotherapeutics.

Antisense microRNA inhibitors (anti-miRs) are chemically modified short ON analogues that are complementary to an endogenous mature miRNA of interest. They function by competitively sequestering the miRNA target in the cytoplasm resulting in miRNA inhibition and consequent derepression of its mRNA target. Although their mechanism of action is not fully understood, anti-miRs were originally thought to stimulate miRNA degradation through an RNase H1-dependent pathway. However, more recent studies have demonstrated that anti-miRs inhibit miRNA function by a steric blocking mechanism and physically associate with Argonaute-bound miRNAs.[72] The consistently poor activity of potent gapmer designs in miRNA assays has led to the hypothesis that the Argonaute-associated miRNA/anti-miR complex may not be accessible to RNase H1.[73-74] Chemical modifications such as 2′-OMe, 2′-*O*-methoxyethyl, 2′-fluoro and LNA have demonstrated effective miRNA targeting during in vitro or in vivo experiments.[75-76]

Luciferase reporter gene assays are commonly employed to evaluate anti-miR potency in miRNA-mediated gene regulation. To investigate whether TMOs can function as miRNA inhibitors *in vitro*, we used a HeLa cell line with two stably integrated luciferase reporters.[77] The *Firefly* luciferase gene (FLuc), under the transcriptional control of a weak upstream constitutive promoter and a downstream poly(A) signal acted as an internal control. A perfectly complementary binding site for hsa-miR-15b-5p was inserted between the *Renilla* luciferase (RLuc) coding sequence and the poly(A) signal located at the multicloning site of psiCHECK-2, (Promega) to transcribe a chimeric *Renilla* mRNA which contains both the *Renilla*-coding sequence and the mir-15b-5p target site (Vector map provided in SI, Section 9). When the reporter plasmid is stably expressed in HeLa cells, *Renilla* luciferase expression is suppressed by endogenous miR-15b-5p, presumably by binding with perfect complementarity to its 3'UTR and subsequently degrading the RLuc mRNA. Potent inhibition of miR-15b-5p using anti-miRs derepresses Renilla gene expression. This increased expression of RLuc can be monitored by measuring the luciferase activity of both RLuc and FLuc using the Dual Luciferase® reporter assay (Promega). Thus, an increase in the production of RLuc correlates with the effectiveness of the anti-miR to bind to endogenous miR-15b, while FLuc provides an internal control to which experimental values can be normalized. The dynamic range of reporter assays are proportional to the copy number of the chosen miRNA target in cells. Inhibiting more abundant miRNAs (~10,000 copies per cell) can result in a larger fold change in RLuc expression compared to miR-15b-5p, which has moderate abundance (~ 800 copies per cell) in HeLa cells.[78]

As a preliminary screen for biological activity, TMOs 3, 4 and 5, designed with varying number and placement of TMO linkages, were screened in the 0.1-1 μM concentration range in the HeLa-15b system described above. A non-targeting control (TMO9) and adequate mock controls (Oligofectamine™ only transfection to control for the effect of transfection reagent on cells) were used. An anti-miR of identical sequence, but exclusively 2'-OMe modified with alternating phosphate and phosphorothioate linkages was tested as positive control. A DNA-pS ON of identical sequence was used as the negative control. All ONs used in this study except TMO9 were full-length reverse complements of endogenous mature miRNA-15b-5p.

To perform the experiment, each ON was transfected via lipofection to 60% confluent HeLa-15b cells (0.1–1 μM of each ON per 96-well). After transfection, the cells were harvested, lysed and analyzed at 24 h. The biological activity was assayed using the Dual-Luciferase® Reporter Assay System (Promega) according to manufacturer's instructions. The ratio of Renilla luminescence to Firefly luminescence (RLuc/FLuc) for ON-treated cells was quantified using a luminometer and this data was normalized to the (RLuc/FLuc) ratio of mock-transfected cells and reported as fold change in RLuc/FLuc with respect to the lipid-only transfection control, which was set to 1. Thus, a taller histogram corresponds to higher RLuc expression due to more efficient miR-15b-5p inhibition. The results of this experiment are shown in SI Chart S1, p. S44.

The DNA-pS control showed poor activity throughout this assay, whereas the chimeric 2'-OMe control and TMO5 showed 6 to 7-fold improved activity within 24 h of transfection. TMO3 (exclusively TMO modified) showed moderate levels of activity, resulting in a 3 to 4-fold change in RLuc expression. Gapmer TMO4 did not show appreciable levels of activity. The non-targeting control TMO9 showed a roughly 2-fold increase in the 0.25–1 μM concentration range implying the presence of off-target effects at high concentrations. The maximum fold-change of RLuc expression was observed for the 2'-OMe control, followed by TMO5 (6 to 7-fold change), and no further increase in activity was observed when the concentrations were increased beyond 100 nM. This could be due to the low to moderate copy numbers of miR-15b-5p in HeLa cells,[78] implying that maximum inhibition might have been achieved at 100 nM. Although a dose-dependent inhibition

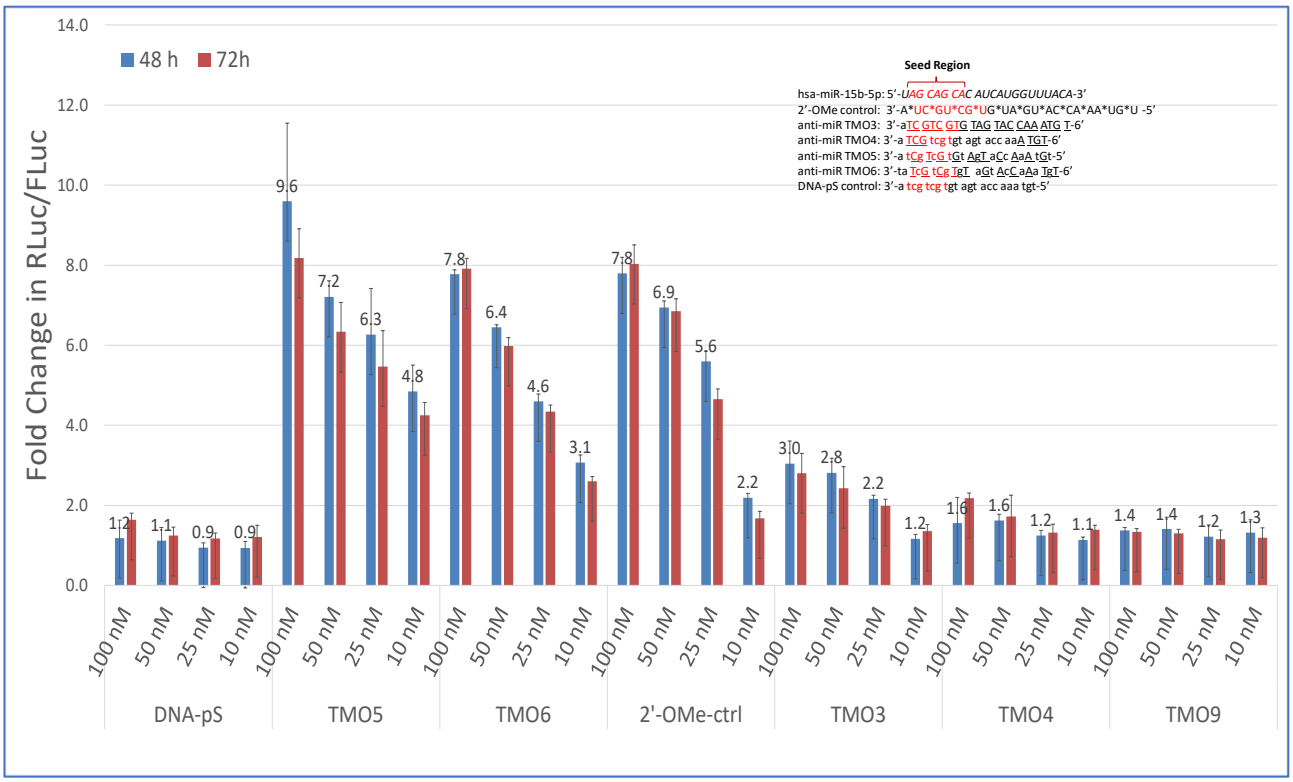

Chart 1 In vitro evaluation of TMOs 3-6 as miR-15b-5p inhibitors. Dose-dependent derepression of RLuc mRNA was observed for TMOs 5 and 6. Anti-miR TMOs 3-6 directed against miR-15b were designed with varying the number and placement of TMO linkages and transfected at concentrations ranging from 10 to 100 nmol/L into HeLa-15b cells stably expressing a psiCHECK-based dual reporter plasmid. Each datapoint represents the mean of four biological replicates per concentration per time point ±SD. Italics: RNA; Uppercase, bold: 2'-OMe sugar; '*' represents position of pS linkages; Uppercase, bold, underline: TMO; lowercase: 2'-deoxynucleotide pS.

could not be observed at higher concentrations, this experiment demonstrated that TMO5 is ~6 fold more active compared to the DNA-pS (negative) control.

In summary, preliminary screening at high ON concentrations indicated that one or more TMO designs may have the potential to be further investigated as anti-miRs. However, it is well known that cellular toxicity, anti-proliferative effects and the manifestation of off-target effects by non-specific binding increases with increasing ON concentration. We therefore attempted to identify the lowest effective doses for the above TMO designs by performing this experiment at a lower concentration range (0.1–100 nM). The transfection protocols were carried out as described earlier.

The DNA-pS anti-miR (negative control) showed poor activity at all concentrations tested. This is can be explained based on its reduced RNA binding affinity (Tm= 56.2°C, Table 2). The 2'-OMe positive control containing 50 % phosphorothioate linkages (predicted T_m = 77.2 °C) effectively inhibited mir-15b-5p at 100 nM concentration; greater than 7-fold change in RLuc expression was observed. This is because the increased binding affinity of 2'-OMe sugars (22-mer) compensates for the decrease in T_m caused by 11 pS linkages (~ -0.5 to -0.7 °C/mod), resulting in a biologically active anti-miR with high target affinity and increased nuclease stability. In comparison, TMO5 and TMO6 (T_m = 74 °C, Table 2) consisting of alternating TMO and DNA-pS linkages also produced a 7-fold change in RLuc expression at 100 nM concentration. Despite its high RNA binding affinity, the exclusively TMO modified anti-miR construct (TMO3, T_m = 74.4 °C, Table 2) was less active and showed only a three-fold inhibition relative to mock-transfected cells. Although the exact reasons remain unclear, this could be attributed to its inability to invade and bind the miRISC complex, poor transfection efficiency or altered intracellular distribution relative to TMO5 and TMO6. Although the gapmer anti-miR TMO4 (T_m = 60.7 °C, Table 2) with TMO wings and a 14-mer DNA-pS gap is capable of eliciting RNase H1 activity, it was not a potent inhibitor miR-15b-5p, presumably due to its poor target binding ability and intrinsic susceptibility to endonucleases.

As shown in Chart 1, the highest miRNA inhibition levels were achieved at 100 nM. A maximal fold-response (~ 8-fold) was detected for TMO5 at 100 nM concentration, 48 h time point. No further increase in activity was observed either at higher TMO5 concentrations (SI Chart S1), or at longer time points for either the TMO-based designs or the 2'-OMe positive control. This is presumably because the dynamic range of the luciferase assay is limited by the moderate copy numbers of miR-15b-5p in HeLa cells.[78]

Anti-miR activities observed at 48h were sustained at 72h, suggesting that TMOs 5 and 6 have sufficient in vitro stability over this time period. Although the 2'-OMe positive control displayed the most potent inhibition in the 25–50 nM range, its activity dropped below that of TMOs 5 and 6 at the lowest tested concentration (10 nM). The higher potency of TMOs 5 and 6 at 10 nM might be due to their enhanced nuclease stability, resulting in the availability of more undegraded anti-miRs over a longer time period.

Additionally, a dose-dependent increase in RLuc expression was observed for alternately modified TMOs 5, 6 and the 2'-OMe control in the 10-100 nM concentration range; between 2 to 5-fold increase in RLuc levels was observed at 10 nM, but more robust RLuc derepression resulted in a 7 to 8-fold inhibition at 100 nM. The DNA-pS control and gapmer TMO4 did not effectively inhibit mir-15b-5p and showed negligible activity during this assay. The non-targeting control TMO9 maintained similar activity levels as the DNA-pS negative control in the 10–100 nM concentration range, suggesting that higher sequence specific binding and fewer off target binding might occur under these conditions.

In summary, suitably designed TMOs can effectively function as miRNA-15b-5p inhibitors in vitro. A dose response study in the 10-100 nM range showed that higher levels of derepression of RLuc mRNA can be achieved with increasing concentrations of TMOs. This experiment further demonstrated that the number and distribution pattern of TMO linkages play a critical role in determining biological activity. This is in agreement with several literature reports which have shown that the placement of high affinity modifications such as 2'-F, 2'-OMe, 2'-MOE, LNA or a non-nucleotide modifier (ZEN linker) wholly dictates the potency of the resulting ON to modulate the activity of miR-21.[74,79] Further experiments are underway to elucidate both the in vitro and in vivo potency of various TMO designs in suitable disease models.

Conclusions

In conclusion, we have successfully developed a chemical synthesis strategy for preparing a new class of synthetic molecules called thiophosphoramidate morpholinos using phosphoramidite chemistry. In contrast to P(V)-based PMO synthesis, the phosphoramidite-based approach lends itself to the easy incorporation of several valuable antisense modifications such as 2'-OMe, 2'-O-MOE, LNA, and others that are commercially available, providing an easy synthetic route to generate an array of previously unexplored drug candidates for oligotherapeutics. A combination of morpholino nucleobases and phosphorothioate linkages resulted in an oligonucleotide construct with exceptional nuclease stability. Based upon a 3'-exonuclease degradation assay using Snake Venom Phosphodiesterase I, TMOs showed minimal degradation over 23 h. They were three times more stable relative to a DNA-pS control. Based on T_m studies, both the number and placement of TMO modifications play a crucial role in dictating binding affinity; while a TMO-DNA-pS gapmer performed poorly, alternately modified TMO-DNA-pS chimeras displayed excellent hybridization affinity towards both DNA and RNA complements. Additionally, it appeared that the placement of rigid morpholino sugars uniformly throughout the ON backbone results in a relatively rigid construct that binds with high affinity to RNA, but not DNA. This lack of flexibility is also suggested by the observation that an exclusively TMO modified ON was RNase H1 inactive. Based on CD spectra, the global helical structure of all TMO/RNA heteroduplexes lies between A and B forms, although the alternately TMO modified chimera displayed prominent A-form bands, approaching a typical RNA/RNA duplex. Preliminary bioactivity screens that test the potency of various TMO designs as anti-miRs showed that some TMO designs may find applications as microRNA inhibitors. In summary, we have demonstrated that TMOs show great promise to be utilized as effective research tools in molecular biology and may have significant potential as novel drug candidates in oligotherapeutics. Efforts are currently underway to further expand the scope of TMO based drug candidates in various therapeutic modalities and elucidate their mechanism of action.

ASSOCIATED CONTENT

Supporting Information. Procedures for the chemical synthesis of 6′-*O*-DMT-phosphorodiamidites and their ^{1}H, ^{13}C, ^{31}P NMR, HRMS data, LCMS characterization of TMO oligonucleotides, analytical RP-HPLC profiles for SVPDE assay, Tm curves, Dual-Luciferase assay data. This material is available free of charge via the Internet at http://pubs.acs.org.

AUTHOR INFORMATION

Corresponding Author

krishna.heera@colorado.edu
marvin.caruthers@colorado.edu

Present Addresses

†Centre of Molecular and Macromolecular Studies, Polish Academy of Sciences, Department of Bioorganic Chemistry, Sienkiewicza 112, 90-363 Łódź, Poland.

Author Contributions

All authors have given approval to the final version of the manuscript.

Funding Sources

This work was funded by the University of Colorado at Boulder.

Notes

The authors declare no competing financial interest.

ACKNOWLEDGMENT

We thank Dr. Annette Erbse and the Shared Instruments Pool of the Department of Biochemistry at the University of Colorado Boulder for the CD spectrometer. We thank Dr. Thomas Lee and the Mass Spectrometry Core Facility for HRMS analysis. The HeLa-15b cell line was a kind gift of miRagen

Therapeutics, Inc. We thank Dr. Katie Robinson and Dr. Christina Dalby for their valuable inputs during the Dual Luciferase assay development.

ABBREVIATIONS

TMO, Thiophosphoramidate Morpholino; RNase H1, Ribonuclease H1; ON, Oligonucleotide; DNA-pS, Phosphorothioate DNA; PMO, Phosphorodiamidate morpholino; CD, Circular Dichroism; OD, Optical Density Units.

REFERENCES

1. Crooke, S. T., *Antisense drug technology: principles, strategies, and applications*. CRC press: 2007.
2. Aartsma-Rus, A.; Jackson, A. L.; Levin, A. A., Mechanisms of oligonucleotide actions. *Oligonucleotide-Based Drugs and Therapeutics*, Ferrari, N.; Seguin, R., Eds. 2018; pp 1-37.
3. Kole, R.; Krainer, A. R.; Altman, S., RNA therapeutics: beyond RNA interference and antisense oligonucleotides. *Nat Rev Drug Discov* **2012,** *11* (2), 125-140.
4. Yin, W.; Rogge, M., Targeting RNA: A transformative therapeutic strategy. *Clinical and Translational Science* **2019,** *12* (2), 98-112.
5. Wu, S. Y.; Lopez-Berestein, G.; Calin, G. A.; Sood, A. K., RNAi therapies: drugging the undruggable. *Science Translational Medicine* **2014,** *6* (240), 240ps7-240ps7.
6. Smith, C. I. E.; Zain, R., Therapeutic Oligonucleotides: State of the Art. *Annual Review of Pharmacology and Toxicology* **2019,** *59* (1), 605-630.
7. Deleavey, Glen F.; Damha, Masad J., Designing chemically modified oligonucleotides for targeted gene silencing. *Chemistry & Biology* **2012,** *19* (8), 937-954.
8. Lim, K. R. Q.; Maruyama, R.; Yokota, T., Eteplirsen in the treatment of Duchenne muscular dystrophy. *Drug Des Devel Ther* **2017,** *11*, 533-545.
9. Heo, Y.-A., Golodirsen: First Approval. *Drugs* **2020,** *80* (3), 329-333.
10. Rodrigues, M.; Yokota, T., An overview of recent advances and clinical applications of exon skipping and splice modulation for muscular dystrophy and various genetic diseases. *Methods Mol Biol* **2018,** *1828*, 31-55.
11. Geary, R. S., Antisense oligonucleotide pharmacokinetics and metabolism. *Expert Opinion on Drug Metabolism & Toxicology* **2009,** *5* (4), 381-391.
12. Amantana, A.; Iversen, P. L., Pharmacokinetics and biodistribution of phosphorodiamidate morpholino antisense oligomers. *Current Opinion in Pharmacology* **2005,** *5* (5), 550-555.
13. Shen, W.; De Hoyos, C. L.; Migawa, M. T.; Vickers, T. A.; Sun, H.; Low, A.; Bell, T. A.; Rahdar, M.; Mukhopadhyay, S.; Hart, C. E.; Bell, M.; Riney, S.; Murray, S. F.; Greenlee, S.; Crooke, R. M.; Liang, X.-h.; Seth, P. P.; Crooke, S. T., Chemical modification of PS-ASO therapeutics reduces cellular protein-binding and improves the therapeutic index. *Nature Biotechnology* **2019,** *37* (6), 640-650.
14. Lightfoot, H.; Schneider, A.; Hall, J., Pharmacokinetics and pharmacodynamics of antisense oligonucleotides. *Oligonucleotide-Based Drugs and Therapeutics: Preclinical and Clinical Considerations for Development* **2018**, 107-136.
15. Summerton, J.; Weller, D., Morpholino antisense oligomers: design, preparation, and properties. *Antisense & nucleic acid drug development* **1997,** *7*, 187-95.
16. Mansoor, M.; Melendez, A., Advances in antisense oligonucleotide development for target identification, validation, and as novel therapeutics. *Gene regulation and systems biology* **2008,** *2*, 275-95.
17. Summerton, J. E.; Weller, D. D.; Stirchak, E. P. Alpha-morpholino ribonucleoside derivatives and polymers thereof. U.S. Patent No. 5,235,033. 10 Aug. 1993.
18. Caruthers, M.; Paul, S. Synthesis of backbone modified morpholino oligonucleotides and chimeras using phosphoramidite chemistry. U.S. Patent Application 16/359,776, July 18, 2019.
19. Seth, P. P.; Ostergaard, M. Morpholino modified oligomeric compounds. WO 2018/165564 A1, 09 March 2018.
20. Palframan, M. J.; Alharthy, R. D.; Powalowska, P. K.; Hayes, C. J., Synthesis of triazole-linked morpholino oligonucleotides via Cu(I) catalysed cycloaddition. *Org Biomol Chem* **2016,** *14* (11), 3112-3119.
21. Zhang, N.; Tan, C.; Cai, P.; Jiang, Y.; Zhang, P.; Zhao, Y., Synthesis and properties of morpholino chimeric oligonucleotides. *Tetrahedron Letters* **2008,** *49* (22), 3570-3573.
22. Zhang, N.; Tan, C.; Cai, P.; Zhang, P.; Zhao, Y.; Jiang, Y., RNA interference in mammalian cells by siRNAs modified with morpholino nucleoside analogues. *Bioorganic & Medicinal Chemistry* **2009,** *17* (6), 2441-2446.
23. Peyrottes, S.; Vasseur, J.-J.; Imbach, J.-L.; Rayner, B., Oligodeoxynucleoside phosphoramidates (P-NH_2): synthesis and thermal stability of duplexes with DNA and RNA targets. *Nucleic Acids Research* **1996,** *24* (10), 1841-1848.
24. Skorski, T.; Perrotti, D.; Nieborowska-Skorska, M.; Gryaznov, S.; Calabretta, B., Antileukemia effect of c-myc N3′→P5′ phosphoramidate antisense oligonucleotides in vivo. *Proceedings of the National Academy of Sciences* **1997,** *94* (8), 3966-3971.
25. Krishna, H.; Jastrzebska, K.; Caruthers, M., Exploring site-specific activation of bis-*N*,*N*'-dialkylaminophosphordiamidites and the synthesis of morpholinophosphoramidate oligonucleotides. *FEBS Letters* **2019,** *593* (13), 1459-1467.
26. Krishna, H.; Jastrzebska, K.; Caruthers, M.; Paul, S.; Veedu Rakesh, N. Thiomorpholino oligonucleotides for the treatment of muscular dystrophy. WO 2019/060522 A3, 2018/09/20, 2019.
27. The notation 6' is used for denoting the position of the terminal hydroxyl group on the morpholino ring.
28. Beaucage, S. L.; Iyer, R. P., The synthesis of modified oligonucleotides by the phosphoramidite approach and their applications. *Tetrahedron* **1993,** *49* (28), 6123-6194.
29. (a)Barone, A. D.; Tang, J. Y.; Caruthers, M. H., In situ activation of bis-dialkylaminophosphines–a new method for synthesizing deoxyoligonucleotides on polymer supports. *Nucleic acids research* **1984,** *12* (10), 4051-4061(b) McBride, L. J.; Caruthers, M. H., An investigation of several deoxynucleoside phosphoramidites useful for synthesizing deoxyoligonucleotides. *Tetrahedron Letters* **1983,** *24* (3), 245-248.
30. Berner, S.; Mühlegger, K.; Seliger, H., Studies on the role of tetrazole in the activation of phosphoramidites. *Nucleic acids research* **1989,** *17* (3), 853-864.
31. Pon, R. T., Enhanced coupling efficiency using 4-dimethylaminopyridine (DMAP) and either tetrazole, 5-(o-nitrophenyl) tetrazole, or 5-(p-nitrophenyl) tetrazole in the solid phase synthesis of oligoribonucleotides by the phosphoramidite procedure. *Tetrahedron Letters* **1987,** *28* (32), 3643-3646.
32. Ora, M.; Murtola, M.; Aho, S.; Oivanen, M., Hydrolytic reactions of 3′-N-phosphoramidate and 3′-N-thiophosphoramidate analogues of thymidylyl-3′,5′-thymidine. *Org Biomol Chem* **2004,** *2* (4), 593-600.
33. Ora, M.; Mattila, K.; Lönnberg, T.; Oivanen, M.; Lönnberg, H., Hydrolytic reactions of diribonucleoside 3′,5′-(3′-N-Phosphoramidates): Kinetics and mechanisms for the P–O and P–N bond cleavage of 3′-Amino-3′-deoxyuridylyl-3′,5′-uridine. *Journal of the American Chemical Society* **2002,** *124* (48), 14364-14372.
34. Krotz, A. H.; McElroy, B.; Scozzari, A. N.; Cole, D. L.; Ravikumar, V. T., Controlled detritylation of antisense

oligonucleotides. *Organic Process Research & Development* **2003,** *7* (1), 47-52.

35. Eckstein, F., Phosphorothioates, essential components of therapeutic oligonucleotides. *Nucleic Acid Ther* **2014,** *24* (6), 374-387.

36. Hudziak, R. M.; Barofsky, E.; Barofsky, D. F.; Weller, D. L.; Huang, S.-B.; Weller, D. D., Resistance of morpholino phosphorodiamidate oligomers to enzymatic degradation. *Antisense and Nucleic Acid Drug Development* **1996,** *6* (4), 267-272.

37. Kurreck, J.; Wyszko, E.; Gillen, C.; Erdmann, V. A., Design of antisense oligonucleotides stabilized by locked nucleic acids. *Nucleic acids research* **2002,** *30* (9), 1911-1918.

38. Prakash, T. P., An overview of sugar-Modified oligonucleotides for antisense therapeutics. *Chemistry & Biodiversity* **2011,** *8* (9), 1616-1641.

39. Uhlmann, E., Peptide nucleic acids (PNA) and PNA-DNA chimeras: From high binding affinity towards biological function. *Biological chemistry* **1998,** *379*, 1045-52.

40. Summerton, J., Morpholino antisense oligomers: the case for an RNase H-independent structural type. *Biochimica et Biophysica Acta (BBA) - Gene Structure and Expression* **1999,** *1489* (1), 141-158.

41. Stein, C. A.; Subasinghe, C.; Shinozuka, K.; Cohen, J. S., Physicochemical properties of phosphorothioate oligodeoxynucleotides. *Nucleic Acids Research* **1988,** *16* (8), 3209-3221.

42. Li, P.; Sergueeva, Z.; Dobrikov, M.; Shaw, B., Nucleoside and oligonucleoside boranophosphates: chemistry and properties. *Chemical reviews* **2007,** *107*, 4746-96.

43. Pongracz, K.; Gryaznov, S., Oligonucleotide N3′→ P5′ thiophosphoramidates: synthesis and properties. *Tetrahedron letters* **1999,** *40* (43), 7661-7664.

44. Wan, W. B.; Migawa, M. T.; Vasquez, G.; Murray, H. M.; Nichols, J. G.; Gaus, H.; Berdeja, A.; Lee, S.; Hart, C. E.; Lima, W. F.; Swayze, E. E.; Seth, P. P., Synthesis, biophysical properties and biological activity of second generation antisense oligonucleotides containing chiral phosphorothioate linkages. *Nucleic acids research* **2014,** *42* (22), 13456-13468.

45. Salazar, M.; Fedoroff, O. Y.; Miller, J. M.; Ribeiro, N. S.; Reid, B. R., The DNA strand in DNA-RNA hybrid duplexes is neither B-form nor A-form in solution. *Biochemistry* **1993,** *32* (16), 4207-4215.

46. Gray, D. M.; Ratliff, R. L.; Vaughan, M. R., Circular dichroism spectroscopy of DNA. In *Methods in Enzymology*, Academic Press: 1992; Vol. 211, pp 389-406.

47. Lesnik, E. A.; Freier, S. M., Relative thermodynamic stability of DNA, RNA, and DNA/RNA hybrid duplexes: relationship with base composition and structure. *Biochemistry* **1995,** *34* (34), 10807-10815.

48. Hung, S.-H.; Yu, Q.; Gray, D. M.; Ratliff, R. L., Evidence from CD spectra that d(purine)-r(pyrimidine) and r(purine)-d(pyrimidine) hybrids are in different structural classes. *Nucleic Acids Research* **1994,** *22* (20), 4326-4334.

49. Zhou, C.; Chattopadhyaya, J., New methylene-bridged hexopyranosyl nucleoside modified oligonucleotides (BHNA): synthesis and biochemical studies. *Arkivoc* **2008,** *2009* (3), pp. 171-186.

50. Clark, C. L.; Cecil, P. K.; Singh, D.; Gray, D. M., CD, absorption and thermodynamic analysis of repeating dinucleotide DNA, RNA and hybrid duplexes $[d/r(AC)]_{12}$·$[d/r(GT/U)]_{12}$ and the influence of phosphorothioate substitution. *Nucleic Acids Research* **1997,** *25* (20), 4098-4105.

51. Lingel, A.; Izaurralde, E., RNAi: finding the elusive endonuclease. *Rna* **2004,** *10* (11), 1675-9.

52. Hollis, T.; Shaban, N. M., Structure and function of RNase H Enzymes. In *Ribonucleases*, Nicholson, A. W., Ed. Springer Berlin Heidelberg: 2011; pp 299-317.

53. Boyer, P. L.; Smith, S. J.; Zhao, X. Z.; Das, K.; Gruber, K.; Arnold, E.; Burke, T. R.; Hughes, S. H., Developing and evaluating inhibitors against the RNase H active site of HIV-1 reverse transcriptase. *Journal of Virology* **2018,** *92* (13), e02203-17.

54. Zamecnik, P. C.; Stephenson, M. L., Inhibition of Rous sarcoma virus replication and cell transformation by a specific oligodeoxynucleotide. *Proceedings of the National Academy of Sciences* **1978,** *75* (1), 280-284.

55. Vickers, T. A.; Koo, S.; Bennett, C. F.; Crooke, S. T.; Dean, N. M.; Baker, B. F., Efficient reduction of target RNAs by small interfering RNA and RNase H-dependent antisense agents: a comparative analysis. *Journal of Biological Chemistry* **2003,** *278* (9), 7108-7118.

56. Furdon, P. J.; Dominski, Z.; Kole, R., RNase H cleavage of RNA hybridized to oligonucleotides containing methylphosphonate, phosphorothioate and phosphodiester bonds. *Nucleic acids research* **1989,** *17* (22), 9193-9204.

57. Rait, V. K.; Shaw, B. R., Boranophosphates support the RNase H cleavage of polyribonucleotides. *Antisense and Nucleic Acid Drug Development* **1999,** *9* (1), 53-60.

58. Miroshnichenko, S. K.; Patutina, O. A.; Burakova, E. A.; Chelobanov, B. P.; Fokina, A. A.; Vlassov, V. V.; Altman, S.; Zenkova, M. A.; Stetsenko, D. A., Mesyl phosphoramidate antisense oligonucleotides as an alternative to phosphorothioates with improved biochemical and biological properties. *Proceedings of the National Academy of Sciences* **2019,** *116* (4), 1229-1234.

59. Noronha, A. M.; Wilds, C. J.; Lok, C.-N.; Viazovkina, K.; Arion, D.; Parniak, M. A.; Damha, M. J., Synthesis and biophysical properties of arabinonucleic acids (ANA): circular dichroic spectra, melting temperatures, and ribonuclease H susceptibility of ANA/RNA hybrid duplexes. *Biochemistry* **2000,** *39* (24), 7050-7062.

60. Verbeure, B.; Lescrinier, E.; Wang, J.; Herdewijn, P., RNase H mediated cleavage of RNA by cyclohexene nucleic acid (CeNA). *Nucleic acids research* **2001,** *29* (24), 4941-4947.

61. Mangos, M. M.; Min, K.-L.; Viazovkina, E.; Galarneau, A.; Elzagheid, M. I.; Parniak, M. A.; Damha, M. J., Efficient RNase H-directed cleavage of RNA promoted by antisense DNA or 2'F-ANA constructs containing acyclic nucleotide inserts. *Journal of the American Chemical Society* **2003,** *125* (3), 654-661.

62. Geary, R. S.; Baker, B. F.; Crooke, S. T., Clinical and preclinical pharmacokinetics and pharmacodynamics of mipomersen (kynamro(®)): a second-generation antisense oligonucleotide inhibitor of apolipoprotein B. *Clin Pharmacokinet* **2015,** *54* (2), 133-146.

63. Nowotny, M.; Gaidamakov, S. A.; Ghirlando, R.; Cerritelli, S. M.; Crouch, R. J.; Yang, W., Structure of Human RNase H1 complexed with an RNA/DNA hybrid: insight into HIV reverse transcription. *Molecular Cell* **2007,** *28* (2), 264-276.

64. Wu, H.; Lima, W. F.; Crooke, S. T., Investigating the structure of Human RNase H1 by site-directed mutagenesis. *Journal of Biological Chemistry* **2001,** *276* (26), 23547-23553.

65. Lima, W. F.; Nichols, J. G.; Wu, H.; Prakash, T. P.; Migawa, M. T.; Wyrzykiewicz, T. K.; Bhat, B.; Crooke, S. T., Structural requirements at the catalytic site of the heteroduplex substrate for Human RNase H1 catalysis. *Journal of Biological Chemistry* **2004,** *279* (35), 36317-36326.

66. Østergaard, M. E.; Nichols, J.; Dwight, T. A.; Lima, W.; Jung, M. E.; Swayze, E. E.; Seth, P. P., Fluorinated nucleotide modifications modulate allele selectivity of SNP-targeting antisense oligonucleotides. *Mol Ther Nucleic Acids* **2017,** *7*, 20-30.

67. Frieden, M.; Christensen, S. M.; Mikkelsen, N. D.; Rosenbohm, C.; Thrue, C. A.; Westergaard, M.; Hansen, H. F.; Ørum, H.; Koch, T., Expanding the design horizon of antisense oligonucleotides with alpha-L-LNA. *Nucleic acids research* **2003,** *31* (21), 6365-6372.

68. Monia, B. P.; Lesnik, E. A.; Gonzalez, C.; Lima, W. F.; McGee, D.; Guinosso, C. J.; Kawasaki, A. M.; Cook, P. D.; Freier, S. M., Evaluation of 2'-modified oligonucleotides containing 2'-deoxy gaps as antisense inhibitors of gene expression. *Journal of Biological Chemistry* **1993,** *268* (19), 14514-14522.

69. Kiełpiński, Ł. J.; Hagedorn, P. H.; Lindow, M.; Vinther, J., RNase H sequence preferences influence antisense oligonucleotide efficiency. *Nucleic Acids Research* **2017,** *45* (22), 12932-12944.

70. Gebert, L. F. R.; MacRae, I. J., Regulation of microRNA function in animals. *Nature Reviews Molecular Cell Biology* **2019,** *20* (1), 21-37.

71. Oliveto, S.; Mancino, M.; Manfrini, N.; Biffo, S., Role of microRNAs in translation regulation and cancer. *World J Biol Chem* **2017,** *8* (1), 45-56.

72. Hogan, D. J.; Vincent, T. M.; Fish, S.; Marcusson, E. G.; Bhat, B.; Chau, B. N.; Zisoulis, D. G., Anti-miRs competitively inhibit microRNAs in Argonaute complexes. *PLoS One* **2014,** *9* (7).

73. Lima, J. F.; Cerqueira, L.; Figueiredo, C.; Oliveira, C.; Azevedo, N. F., Anti-miRNA oligonucleotides: a comprehensive guide for design. *RNA Biol* **2018,** *15* (3), 338-352.

74. Davis, S.; Lollo, B.; Freier, S.; Esau, C., Improved targeting of miRNA with antisense oligonucleotides. *Nucleic acids research* **2006,** *34* (8), 2294-2304.

75. Ishida, M.; Selaru, F. M., miRNA-Based therapeutic strategies. *Current Pathobiology Reports* **2013,** *1* (1), 63-70.

76. Esau, C.; Davis, S.; Murray, S. F.; Yu, X. X.; Pandey, S. K.; Pear, M.; Watts, L.; Booten, S. L.; Graham, M.; McKay, R.; Subramaniam, A.; Propp, S.; Lollo, B. A.; Freier, S.; Bennett, C. F.; Bhanot, S.; Monia, B. P., miR-122 regulation of lipid metabolism revealed by in vivo antisense targeting. *Cell Metabolism* **2006,** *3* (2), 87-98.

77. This cell line was a kind gift from miRagen Therapeutics, Inc.

78. Hullinger, T. G.; Montgomery, R. L.; Seto, A. G.; Dickinson, B. A.; Semus, H. M.; Lynch, J. M.; Dalby, C. M.; Robinson, K.; Stack, C.; Latimer, P. A.; Hare, J. M.; Olson, E. N.; Rooij, E. v., Inhibition of miR-15 protects against cardiac ischemic injury. *Circulation Research* **2012,** *110* (1), 71-81.

79. Lennox, K. A.; Owczarzy, R.; Thomas, D. M.; Walder, J. A.; Behlke, M. A., Improved performance of anti-miRNA oligonucleotides using a novel non-nucleotide Modifier. *Mol Ther Nucleic Acids* **2013,** *2* (8), e117-e117.

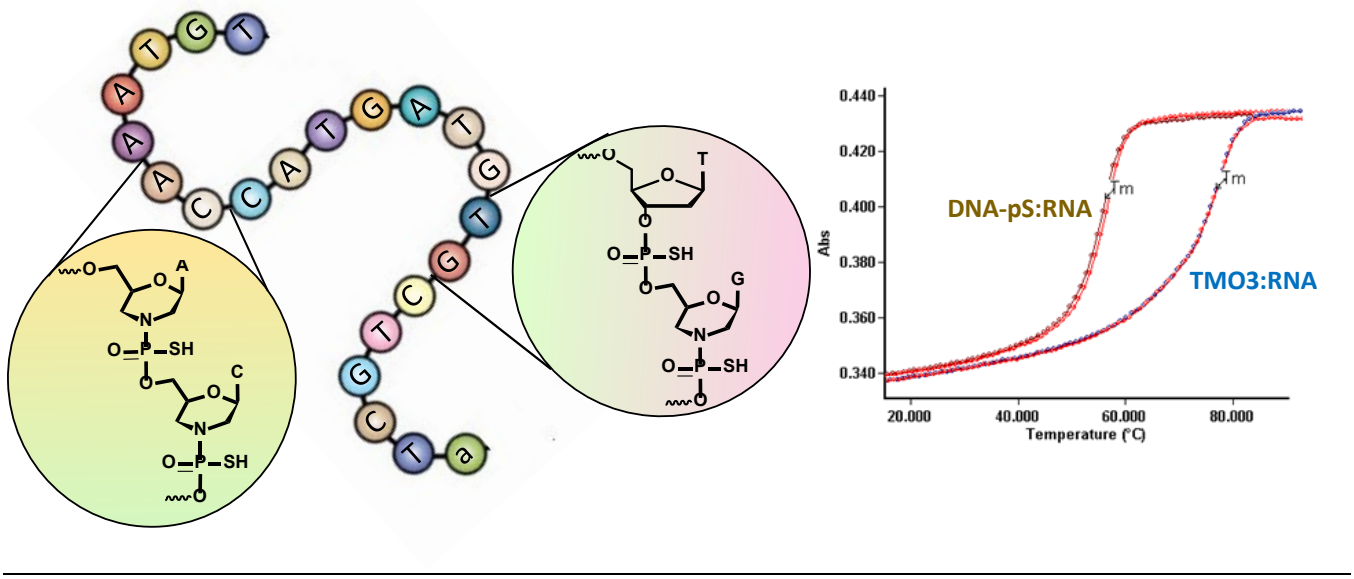
DNA-pS:RNA
TMO3:RNA
Tm
Tm
Abs
Temperature (°C)
0.440
0.420
0.400
0.380
0.360
0.340
20.000
40.000
60.000
80.000

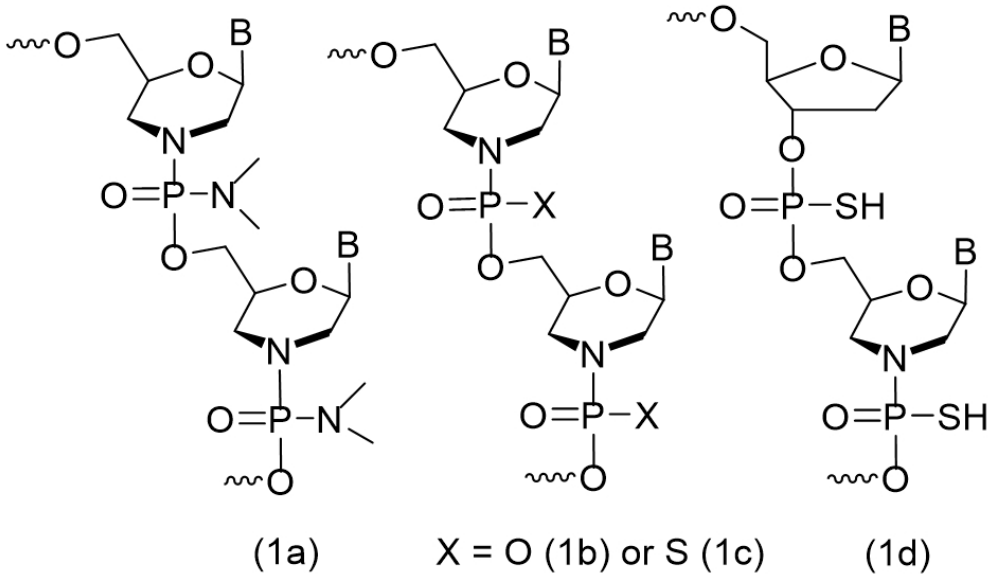

Figure 1 Chemical representation of phosphorodiamidate morpholino (PMO) (1a), phosphoramidate morpholino (1b), thiophosphoramidate morpholino TMO (1c) and TMO-DNA-pS chimeras (1d).

39x30mm (600 x 600 DPI)

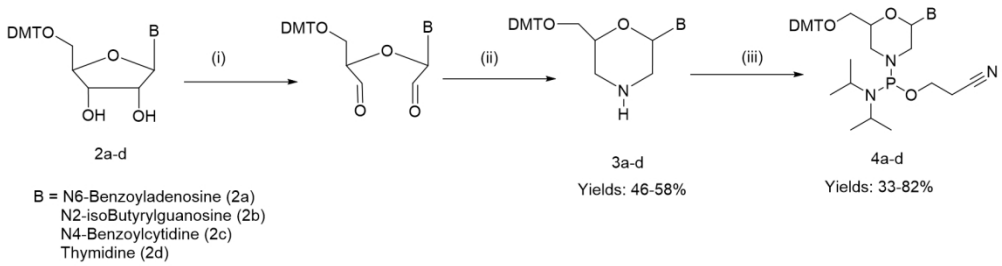

Scheme 1 Chemical synthesis of phosphorodiamidite synthons 4a-d. Reagents and conditions: (i) NaIO4 (1.2 equiv.), anhydrous methanol; (NH4)2B2O7 (1.2 equiv.), 6 h (ii) NaCNBH3 (2.0 equiv);CH3COOH (2.0 equiv.), 16h (iii) (OCH2CH2CN)P[N(iPr)2]2 (1.2 equiv.), 5-Ethylthio-1H-Tetrazole (0.5 equiv.),CH2Cl2, 30 min.

76x30mm (600 x 600 DPI)

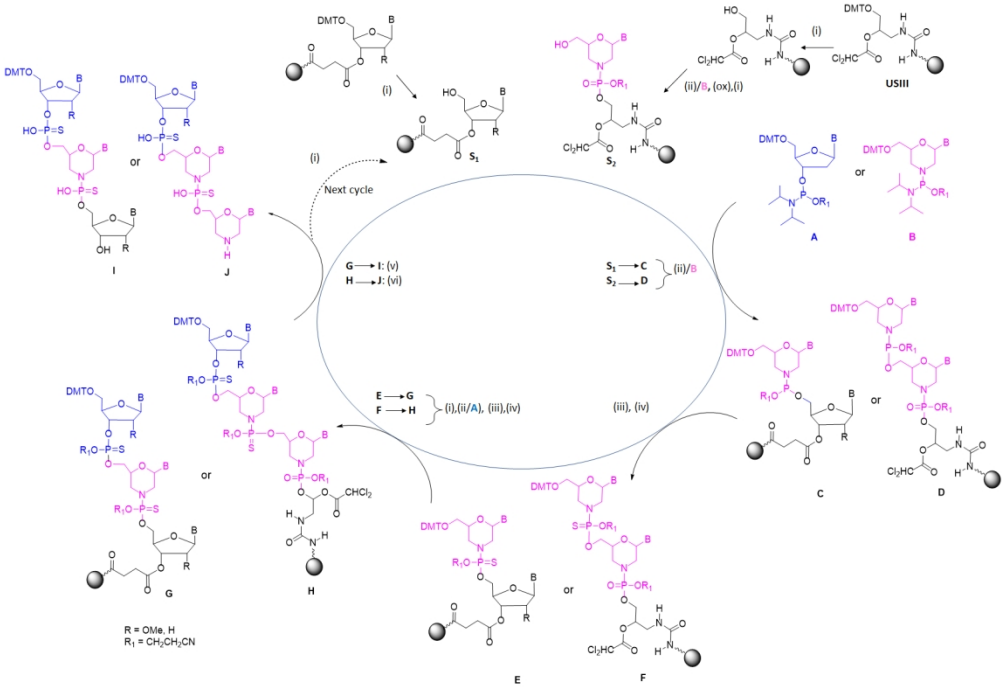

Figure 2 Solid-phase Synthesis of TMO and TMO-DNA-pS Chimeras; Reagents: (i) Detritylation: 3% trichloroacetic acid/CH2Cl2 (ii) Condensation: 0.12M 5-Ethylthio-1H-tetrazole/CH3CN, 600s wait (iii) Sulfurization: 0.05 M DDTT/pyridine/CH3CN (iv) Capping: Ac2O/pyridine/THF; 1-Methylimidazole/CH3CN (v) Deprotection: 28% aqueous ammonia, 55 oC, 16 h or (vi) Deprotection: 2M ammonia in methanol, 60 min, followed by 28 % aqueous ammonia, 55 oC, 16 h. Amidites A, B are color-coded to simplify the cycle.

75x53mm (600 x 600 DPI)

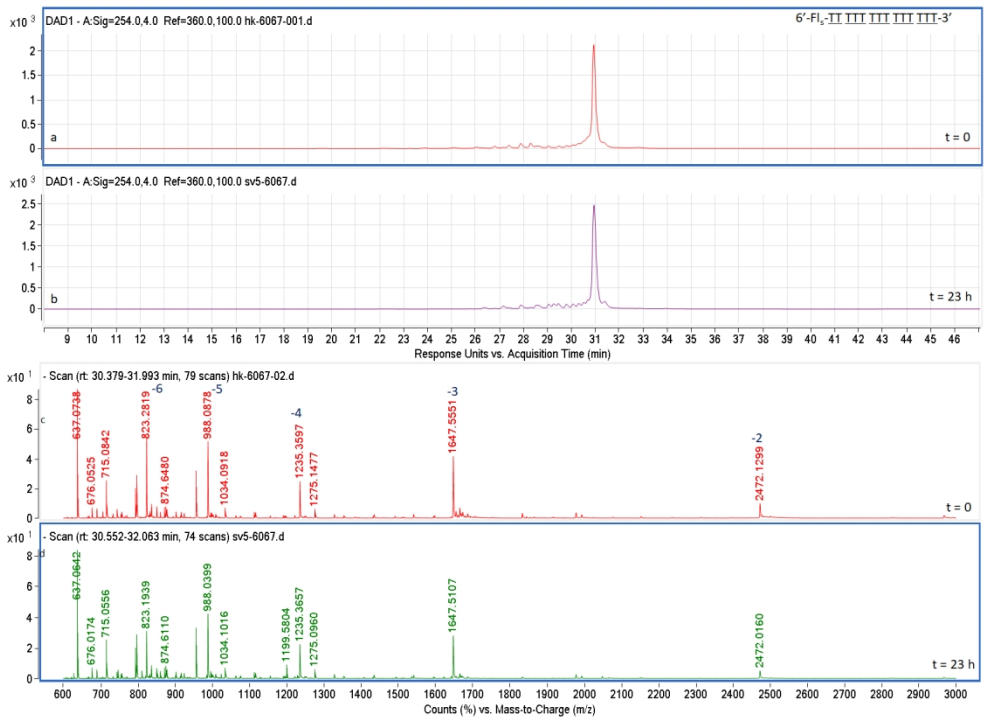

Figure 3 LCMS Analysis of TMO8 During the SVPDE Assay. Analytical RP-HPLC Fractions corresponding to TMO8 were collected at various time points during SVPDE treatment (SI Figures S18-S23: Collected fractions with Rt = 13-16 min). Figure 3(a, b) show the LCMS UV profiles corresponding to TMO8 after SVPDE treatment (t = 0, 23 h). Figure 3(c, d) compare the m/z data at t=0 (untreated) and t =23 h.

72x52mm (600 x 600 DPI)

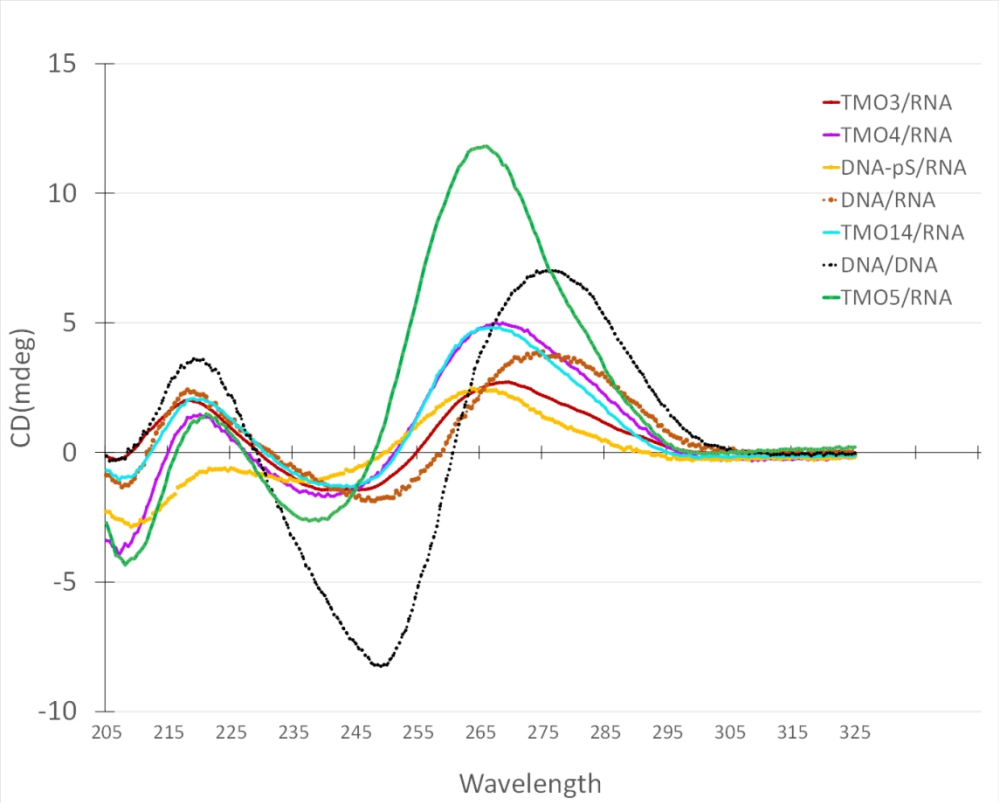

Figure 4 Circular Dichroism of TMOs 3, 4, 5 and 14 relative to DNA-pS/RNA, DNA/RNA and DNA/DNA as controls. An example for an A-form RNA/RNA control duplex is provided in SI Figure S34.

58x47mm (600 x 600 DPI)

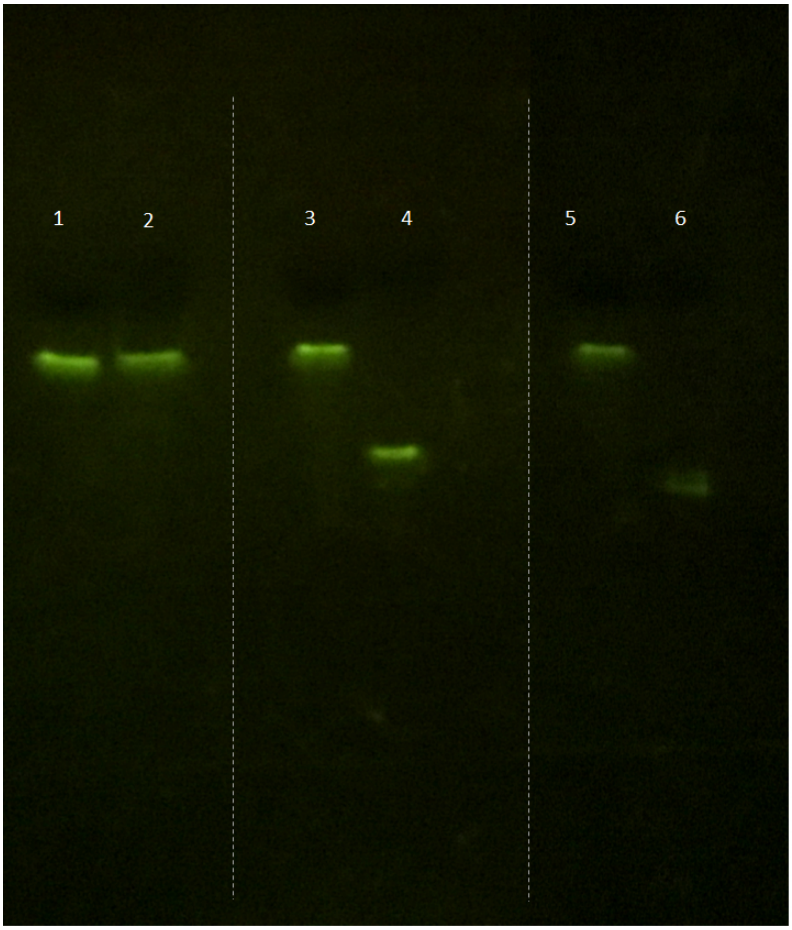

Figure 5 Gel electrophoresis images of 5'-Fl-RNA duplexes of TMOs 3, 4 and control DNA-pS following the E. Coli RNase H1 assay. Fluorescence arises only from intact 5'-Fl-RNA or its degraded fragments. Lane 1: TMO3/RNA duplex ctrl; Lane 2: TMO3/RNA duplex + RNase H1; Lane 3: TMO4/RNA duplex ctrl; Lane 4: TMO4/RNA duplex + RNase H1; Lane 5: DNA-pS/RNA duplex ctrl; Lane 6: DNA-pS/RNA duplex + RNase H1.

38x35mm (600 x 600 DPI)

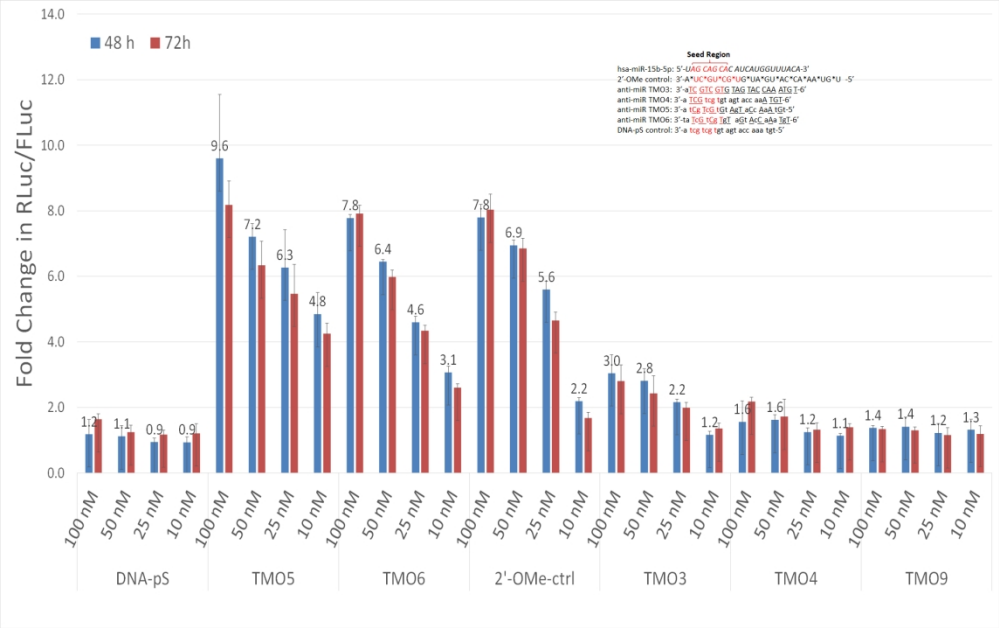

Chart 1 In vitro evaluation of TMOs 3-6 as miR-15b-5p inhibitors. Dose-dependent derepression of RLuc mRNA was observed for TMOs 5 and 6. Anti-miR TMOs 3-6 directed against miR-15b were designed with varying the number and placement of TMO linkages and transfected at concentrations ranging from 10 to 100 nmol/L into HeLa-15b cells stably expressing a psiCHECK-based dual reporter plasmid. Each datapoint represents the mean of four biological replicates per concentration per time point ±SD. Italics: RNA; Uppercase, bold: 2’-OMe sugar; ‘*’ represents position of pS linkages; Uppercase, bold, underline: TMO; lowercase: 2’-deoxynucleotide pS.

86x54mm (600 x 600 DPI)

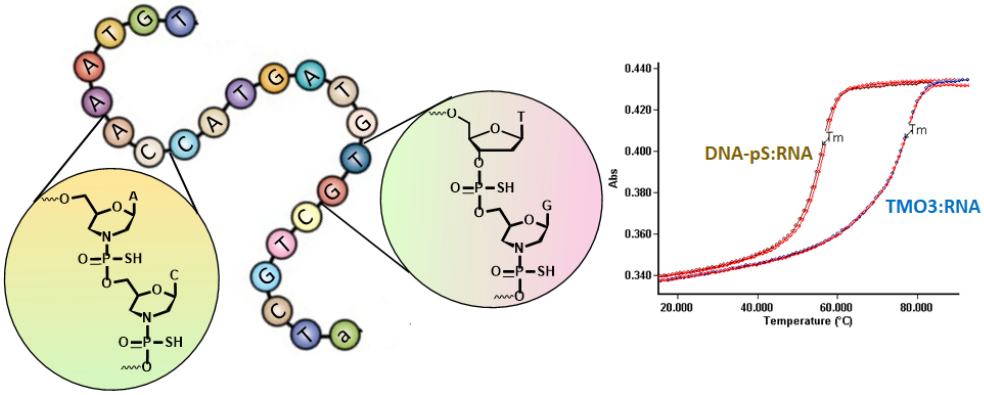

Art Work (Table of Contents)

41x30mm (600 x 600 DPI)